Elsevier Editorial System(tm) for European Journal of Mechanics - A/Solids
Manuscript Draft

Manuscript Number:

Title: A FULL 3D DISCRETE ELEMENT MODEL FOR THE NONLINEAR BEHAVIOUR OF MASONRY WALLS

Article Type: Full length article

Keywords: Masonry walls; 3D discrete element model; Mohr-Coulomb yield criterion

Corresponding Author: Dr. Daniele Baraldi, Ph.D.

Corresponding Author's Institution: University IUAV of Venezia

First Author: Daniele Baraldi, Ph.D.

Order of Authors: Daniele Baraldi, Ph.D.; Antonella Cecchi, Prof.

Abstract: This paper presents and validates a non commercial discrete element model code for performing nonlinear analysis of one leaf masonry assemblages with regular texture, in three dimensional field. Hypotheses of rigid blocks and joints modelled as interfaces are adopted for representing historic masonry behaviour, characterized by dry joints or weak mortar joints having negligible size with respect to block size. Masonry elastic and inelastic behaviour is concentrated at joints by defining their normal, shear, bending and torsion stiffness and strength, adopting a Mohr-Coulomb criterion for restraining interface actions. The proposed model is an extension to the nonlinear field of an existing code, moreover nonlinear analyses follow an effective approach introduced by authors for the in plane case, based on the determination and update of the stiffness matrix of the masonry assemblage during the incremental analysis, accounting for damage.
A numerical experimentation is performed for determining limit load multipliers and collapse mechanisms of several masonry walls subject to in plane actions generated by self-weight and out of plane actions that may cause tilting or toppling of masonry assemblage portions. Dry and mortar joints are considered and existing case studies are adopted for calibrating the proposed model and evaluating its effectiveness.

Author Agreement

Università Iuav di Venezia

Dorsoduro 2206 Terese
30123 Venezia
f. +39 041 257 1297

DIPARTIMENTO DI
ARCHITETTURA COSTRUZIONE
CONSERVAZIONE

Antonella Cecchi direttore

Venezia, 25/05/2016

Dear Editor,

Antonella Cecchi and myself would like to submit the manuscript: “A full 3D discrete element model for the nonlinear behaviour of masonry walls" for possible publication on European Journal of Mechanics - A/Solids.
This is an original paper which has neither previously, nor simultaneously, in whole or in part been submitted anywhere else, in English or in any other language, without the written consent of the publisher.

Daniele Baraldi
University IUAV of Venezia
DACC - Departement of Architecture Construction Conservation
Dorsoduro 2206, ex convento Terese
30123 Venezia - Italy
tel: +39 041 257 1298
fax: +39 041 257 1282
e-mail: danielebaraldi@iuav.it

Best regards,
Daniele Baraldi.

Venezia, 25 may 2016

Cover Letter

I
U
A
V

Università Iuav di Venezia

Dorsoduro 2206 Terese
30123 Venezia
f. +39 041 257 1297

DIPARTIMENTO DI
ARCHITETTURA COSTRUZIONE
CONSERVAZIONE

Antonella Cecchi direttore

Venezia, 25/05/2016

Dear Editor,

Antonella Cecchi and myself would like to submit the manuscript: “A full 3D discrete element model for the nonlinear behaviour of masonry walls" for possible publication on European Journal of Mechanics - A/Solids.
Do not hesitate to contact me at the following address:

Daniele Baraldi
University IUAV of Venezia
DACC - Departement of Architecture Construction Conservation
Dorsoduro 2206, ex convento Terese
30123 Venezia - Italy
tel: +39 041 257 1298
fax: +39 041 257 1282
e-mail: danielebaraldi@iuav.it

Best regards,
Daniele Baraldi.

Venezia, 25 may 2016

Highlights

- A simple and effective model for 3D analysis of regular masonry in nonlinear fields is presented.
- 3D DEM is based on rigid blocks and elastic-plastic joints with a Mohr-Coulomb yield criterion.
- 3D DEM allows to obtain collapse mechanisms, limit loads and incremental curves of masonry walls.
- 3D DEM is in agreement with existing experimental and numerical results with dry and mortar joints.

A FULL 3D DISCRETE ELEMENT MODEL FOR THE NONLINEAR BEHAVIOUR OF MASONRY WALLS

Daniele Baraldi[1*] and Antonella Cecchi[2]

Department of Architecture, Construction and Conservation, Università IUAV di Venezia
Dorsoduro 2206, 30123, Venezia, Italy
[1]e-mail: danielebaraldi@iuav.it
Tel. +39 041 257 1298
[2]e-mail: cecchi@iuav.it
Tel. +39 041 257 1297

[*] corresponding author

Keywords: Masonry walls, 3D discrete element model, Mohr-Coulomb yield criterion.

Abstract

This paper presents and validates a non commercial discrete element model code for performing nonlinear analysis of one leaf masonry assemblages with regular texture, in three dimensional field. Hypotheses of rigid blocks and joints modelled as interfaces are adopted for representing historic masonry behaviour, characterized by dry joints or weak mortar joints having negligible size with respect to block size. Masonry elastic and inelastic behaviour is concentrated at joints by defining their normal, shear, bending and torsion stiffness and strength, adopting a Mohr-Coulomb criterion for restraining interface actions. The proposed model is an extension to the nonlinear field of an existing code, moreover nonlinear analyses follow an effective approach introduced by authors for the in plane case, based on the determination and update of the stiffness matrix of the masonry assemblage during the incremental analysis, accounting for damage.

A numerical experimentation is performed for determining limit load multipliers and collapse mechanisms of several masonry walls subject to in plane actions generated by self-weight and out of plane actions that may cause tilting or toppling of masonry assemblage portions. Dry and mortar joints are considered and existing case studies are adopted for calibrating the proposed model and evaluating its effectiveness

1 INTRODUCTION

Earthquake actions are one of the main causes of collapse of masonry structures, hence the assessment of their seismic performance remains a challenging task in the structural analysis field of research. As well known, the two main seismic induced damages and collapse modes of masonry walls are in plane and out of plane collapse mechanisms. The former are responsible for extended in plane shear deformations and cracks, while the latter may cause the tilting of entire wall portions, depending on wall restraints, leading eventually to the partial or total collapse of the construction. These collapse mechanisms were observed in past earthquakes and recurring mechanism types have been frequently found. Rondelet (1802) was the first to show several fundamental out of plane mechanism types, whereas the more recent research work of Giuffré (1991) has brought back to light the out of plane collapse behaviour of masonry. The description of out of plane mechanisms related to seismic actions has been recently described by several authors and mechanisms description by means of numerical and analytical models have been done and are still being developed (de Felice and Giannini, 2001; D'Ayala and Speranza, 2003).

Masonry is a heterogeneous structural material obtained by composition of natural or artificial blocks connected by dry or mortar joints following a regular or irregular arrangement.

The behaviour of masonry is frequently modelled numerically in order to assess the structural behaviour of masonry buildings or building portions; for this purpose several types of models may be adopted. On one hand, models may consider material heterogeneity and microstructure by means of heterogeneous Finite Element (FE) Models or Discrete Element (DE) Models (or DEMs), in particular for performing analysis at micro- or meso-scale level. On the other hand, masonry may be modelled as a homogeneous material by means of FE models, for performing analysis at macro scale level or modelling a masonry structure as a whole. Moreover, different analysis types may be performed such as limit analysis or incremental/pushover analysis. For instance, an overview of the methods for modelling masonry structures may be found in the work of Smoljanović et al. (2013) and a deep literature review related to masonry out of plane behaviour and to the corresponding numerical models has been recently done by Ferreira et al. (2015).

Focusing on discrete models, the simplest DEM is based on the assumptions of rigid blocks and joints modelled as interfaces. These assumptions may be suitable for modelling historical masonry, characterized by block stiffness larger than joint stiffness, allowing to assume blocks as rigid bodies, and characterized by a negligible joint thickness if compared with

block size, especially in case of dry joints, allowing to model joints as interfaces. Moreover, a frictional interface behaviour is often adopted for modelling contacts between blocks. Discrete models with rigid blocks were adopted in the past by many authors for studying masonry out of plane behaviour in linear and nonlinear fields, given that the hypotheses adopted allow to perform both traditional elastic or pushover analysis (Casolo, 2000; Cecchi and Sab, 2004; Stefanou et al., 2008) and, more frequently, limit analysis (Livesley, 1978, 1992; Baggio and Trovalusci, 1993; 1998; Gilbert and Melbourne, 1994; Ferris and Tin-Loi, 2001; Gilbert et al., 2003; Orduña and Lourenço, 2005a).. In particular, Cecchi and Sab (2004) defined a simple and effective DEM for studying the three-dimensional behaviour of masonry panels with a small computational effort due to the small number of degrees of freedom (DOFs) involved, represented by block translations and rotations.

It is worth noting that in this field of analysis a lot of experimental campaigns have been performed for assessing the out of plane behaviour and strength of masonry and in order to validate less or more accurate numerical models. Tests were performed both in case of mortar joints (West et al., 1977; Chee Liang, 1996; van der Pluijm, 1999; Griffith et al., 2004; Milani et al., 2007) and in case of dry joints (Portioli et al., 2013; Restrepo-Vélez et al., 2013; Casapulla and Portioli, 2015, 2016), with particular attention, in the latter case, to the frictional behaviour of dry joints in case of torsion.

In this work, the original three-dimensional discrete element model (3D DEM) introduced by Cecchi and Sab (2004) in the linear elastic field for one leaf regular masonry, is extended to the field of collapse analysis by assuming a Mohr-Coulomb yield criterion for defining the elastic limit of interface actions and an elastic-perfectly plastic relationship between interface forces and interface relative translations and rotations is assumed. With this aim, a simple set of nonlinear springs based on interface discretization is introduced for simulating interface normal and shear stresses generated by interface relative translations and rotations, in order to obtain a yield criterion in terms of interface actions. The resulting restraints to interface actions turn out to be coincident with the results obtained analytically by Orduña and Lourenço (2005a), as expected; moreover, parametric analyses are carried on for obtaining simple expressions for interface shear strength and combined shear-torsion strength, that are adopted for the analysis of masonry panels instead of using the approximated domains described by Orduña and Lourenço (2005a). Nonlinear incremental/pushover analyses are performed both at interface level and at panel size level. In the second case, a static solution approach characterized by the determination of the stiffness matrix of the masonry

assemblage is adopted, following and extending the procedure introduced by authors for the nonlinear incremental analysis of masonry walls in plane loaded (Baraldi and Cecchi, 2016a), showing the better computational performance of the proposed method instead of adopting a molecular dynamics algorithm. Moreover, stiffness matrix determination has already been adopted for performing in and out of plane modal analysis of masonry walls (Baraldi et al, 2016; Baraldi and Cecchi, 2016c). Several numerical experiments of masonry panels out of plane loaded are carried on in order to validate the proposed nonlinear DEM with respect to existing numerical and laboratory results. For first, numeric out of plane tests performed by Orduña and Lourenço (2005b) are reproduced. Then, the experimental campaign on scaled masonry-like specimens performed by Restrepo Vélez et al. (2014) is taken in consideration and several cases are reproduced with the proposed nonlinear DEM. Finally, the laboratory experiments carried out by Chee Liang (1996) are considered for evaluating nonlinear DEM effectiveness in case of walls with mortar joints. Analyses performed with the proposed DEM allow to obtain ultimate loads together with the corresponding collapse mechanisms and, differently than limit analysis, load-displacement incremental curves are obtained as a further information on panel behaviour. In general, the proposed numerical solution method turns out to be effective for the determination of limit loads and of the corresponding out of plane collapse mechanisms, with a small computational effort represented by the determination of the updated stiffness matrix of the masonry assemblage during each step of the incremental analyses.

2 THREE DIMENSIONAL DISCRETE MODEL

A regular one leaf masonry with running bond periodic pattern is considered; the generic block $B_{i,j}$ is in contact with six neighbours by means of six interfaces or joints S_{k_1,k_2}, with k_1, $k_2 = \pm 1$ for horizontal interfaces and $k_1 = \pm 2$, $k_2 = 0$, for vertical interfaces (Figure 1a). Block dimensions are: *a* (height), *b* (width) and *s* (thickness) and the periodic pattern is characterized by horizontal interfaces having width equal to block half width.

Assuming rigid block hypothesis, the displacement of the generic block $B_{i,j}$ is represented by a rigid body motion referred to the translation of its centre and the rotation with respect to its centre:

$$\mathbf{u}^{i,j}(\mathbf{y}) = \mathbf{u}^{i,j} + \boldsymbol{\Omega}^{i,j}(\mathbf{y} - \mathbf{y}^{i,j}). \tag{1}$$

Where $\mathbf{y}^{i,j}$ is the position of block centre in the Euclidean space: $\mathbf{y}^{i,j} = i\,(b/2)\,\mathbf{e}_1 + j\,a\,\mathbf{e}_2$. Considering the 3D case, $\mathbf{u}^{i,j} = \{u_1^{i,j}\ u_2^{i,j}\ u_3^{i,j}\}^T$ is the translation vector of $B_{i,j}$ and $\mathbf{\Omega}^{i,j}$ is its rotation skew tensor collecting block rotations with respect to block local coordinate axes:

$$\mathbf{\Omega}^{i,j} = \begin{bmatrix} 0 & -\omega_3^{i,j} & \omega_2^{i,j} \\ \omega_3^{i,j} & 0 & -\omega_1^{i,j} \\ -\omega_2^{i,j} & \omega_1^{i,j} & 0 \end{bmatrix} \tag{2}$$

In and out of plane block translations and rotations (Figure 1b) may be collected in $\mathbf{q}^{i,j} = \{u_1^{i,j}\ u_2^{i,j}\ u_3^{i,j}\ \omega_1^{i,j}\ \omega_2^{i,j}\ \omega_3^{i,j}\}^T$. Following the procedure described by Cecchi and Sab (2004), relative translations and rotations of two adjacent blocks $B_{i,j}$ and $B_{i+k_1,j+k_2}$ may be defined as function of block translations and rotations:

$$\begin{aligned}
d_1^{k_1,k_2} &= u_1^{i+k_1,j+k_2} - u_1^{i,j} + k_2 a(\omega_3^{i+k_1,j+k_2} + \omega_3^{i,j})/2, \\
d_2^{k_1,k_2} &= u_2^{i+k_1,j+k_2} - u_2^{i,j} - k_1(b/2)(\omega_3^{i+k_1,j+k_2} + \omega_3^{i,j})/2, \\
d_3^{k_1,k_2} &= u_3^{i+k_1,j+k_2} - u_3^{i,j} + k_1(b/2)(\omega_2^{i+k_1,j+k_2} + \omega_2^{i,j})/2 - k_2 a(\omega_1^{i+k_1,j+k_2} + \omega_1^{i,j})/2, \\
\delta_1^{k_1,k_2} &= \omega_1^{i+k_1,j+k_2} - \omega_1^{i,j}, \\
\delta_2^{k_1,k_2} &= \omega_2^{i+k_1,j+k_2} - \omega_2^{i,j}, \\
\delta_3^{k_1,k_2} &= \omega_3^{i+k_1,j+k_2} - \omega_3^{i,j}.
\end{aligned} \tag{3}$$

that may be collected in $\mathbf{d}^{k_1,k_2} = \{d_1^{k_1,k_2}\ d_2^{k_1,k_2}\ d_3^{k_1,k_2}\ \delta_1^{k_1,k_2}\ \delta_2^{k_1,k_2}\ \delta_3^{k_1,k_2}\}^T$. It is worth noting that in order to better highlight the relation between relative displacements and block translations and rotations, the above expressions may be written in matrix form as $\mathbf{d}^{k_1,k_2} = \mathbf{H}^{k_1,k_2}\mathbf{q}^{k_1,k_2}$, where $\mathbf{q}^{k_1,k_2}$ collects translations and rotations of two adjacent blocks: $\mathbf{q}^{k_1,k_2} = \{(\mathbf{q}^{i,j})^T\ (\mathbf{q}^{i+k_1,j+k_2})^T\}^T$, and $\mathbf{H}^{k_1,k_2}$ may be defined as interface 'compatibility' matrix (Ferris and Tin-Loi, 2003), that is a triangular matrix collecting, following Equation (3), the relative distances between the centres of the blocks considered. Such distances are equal to *b*/2 and *a* due to the regular pattern considered, but the expression may be extended to generic relative distances dy_1 and dy_2 in case of different patterns, further details are given in appendix.

The interactions between two adjacent blocks $B_{i,j}$ and $B_{i+k_1,j+k_2}$ through a generic interface S_{k_1,k_2} are represented by interface stresses $\boldsymbol{\sigma}$ that are related to the relative displacement and rotations between adjacent blocks by means of a constitutive relation $\boldsymbol{\sigma}\mathbf{n} = \mathbf{K}\,\mathbf{d}$, neglecting for simplicity apex k_1,k_2. Here $\boldsymbol{\sigma}$ is the stress tensor, $\mathbf{n}$ is the normal vector to the generic interface and $\mathbf{K}$ is the interface stiffness matrix. Assuming initially the hypothesis of elastic

interface behaviour, the interface stiffness matrix **K** may be detailed for horizontal and vertical case: $\mathbf{K}_h = \text{diag}\{k_t\ k_n\ k_t\ k_r\ k_t\ k_r\}$ and $\mathbf{K}_v = \text{diag}\{k_n\ k_t\ k_t\ k_t\ k_r\ k_r\}$, collecting tangential (k_t), normal (k_n) and rotational (k_r) stiffness of the interface. It is worth noting that rotational stiffness assumes the same value of normal stiffness ($k_r = k_n$), but it is defined by a different variable given that in the following description of interface nonlinear behaviour it will be necessary to distinguish between nonlinear behaviour of normal forces with respect to that of bending moments. Assuming mortar joints with an isotropic and elastic behaviour, interface stiffness values are function of mortar elastic modulus E^m and Poisson ratio ν^m (Cecchi and Sab, 2004). The elastic energy of the interface is determined by defining the product of interface stresses and interface relative displacements:

$$\Pi_{k_1,k_2} = \frac{1}{2}\int_{S_{k_1,k_2}} \boldsymbol{\sigma}^T \mathbf{d}\, dS = \frac{1}{2}\int_{S_{k_1,k_2}} \mathbf{d}^T \mathbf{K}\, \mathbf{d}\, dS = \frac{1}{2}\mathbf{d}^T(\mathbf{KA})\,\mathbf{d} = \frac{1}{2}\mathbf{d}^T \bar{\mathbf{K}}\, \mathbf{d}, \tag{4}$$

where apex k_1,k_2 for vectors and matrices is omitted for simplicity, **A** is the generic (diagonal) matrix of area and inertias of the interface, that may be detailed for horizontal and vertical cases: $\mathbf{A}_h = \text{diag}\{S_h\ \ S_h\ \ S_h\ \ I_{h1}\ \ (I_{h1}+I_{h3})\ \ I_{h3}\}$, $\mathbf{A}_v = \text{diag}\{S_v\ \ S_v\ \ S_v\ \ (I_{v2}+I_{v3})\ \ I_{v2}\ \ I_{v3}\}$, with

$$\begin{aligned} &S_h = b\,s/2, \quad I_{h1} = b\,s^3/24, \quad I_{h3} = b^3 s/96, \\ &S_v = a\,s, \quad I_{v2} = a\,s^3/12, \quad I_{v3} = a^3 s/12. \end{aligned} \tag{5}$$

Expressions (I_{h1}+I_{h3}) and (I_{v2}+I_{v3}) represent interface polar inertia for horizontal and vertical case, respectively. Interface forces and moments may be obtained by differentiating the expression of interface elastic energy in Equation (4) with respect to each block displacement component. Such unknown forces $f_1^{k_1,k_2}$, $f_2^{k_1,k_2}$, $f_3^{k_1,k_2}$ and moments $m_1^{k_1,k_2}$, $m_2^{k_1,k_2}$, $m_3^{k_1,k_2}$ may be collected in $\mathbf{f}^{k_1,k_2} = \{f_1^{k_1,k_2}\ \ f_2^{k_1,k_2}\ \ f_3^{k_1,k_2}\ \ m_1^{k_1,k_2}\ \ m_2^{k_1,k_2}\ \ m_3^{k_1,k_2}\}^T$ and it can be easily demonstrated that $\mathbf{f}^{k_1,k_2} = \bar{\mathbf{K}}^{k_1,k_2}\mathbf{d}^{k_1,k_2}$. Extending Equation (4) to the entire masonry assemblage (i.e. masonry panel), the total elastic energy Π is obtained and the subsequent equilibrium equation for the assemblage subject to generic in and out of plane actions $\mathbf{F}^{ext}$ is:

$$\mathbf{F}^{ext} = \partial\Pi / \partial\mathbf{q}^{panel} = \mathbf{K}^{panel}\mathbf{q}^{panel}, \tag{6}$$

where $\mathbf{q}^{panel}$ collects block displacements and rotations of the entire panel. Equation (6) may be solved by adopting a molecular dynamics algorithm (Cecchi and Sab, 2004) or directly by explicitly defining the stiffness matrix of the entire assemblage $\mathbf{K}^{panel}$, joining together the procedures already proposed by authors (Baraldi et al., 2015; Baraldi and Cecchi, 2016a and Baraldi et al., 2016) for the in and out of plane cases, respectively, and used separately in the

field of in and out of plane modal analysis of masonry panels and in the field of nonlinear analysis of masonry panels in plane loaded. In particular, the determination of panel stiffness matrix is based on the definition of a 'compatibility' matrix at panel level $\mathbf{H}^{panel}$ obtained by assembling matrices $\mathbf{H}^{k_1,k_2}$ over the panel and that relates relative displacements of the entire panel $\mathbf{d}^{panel}$ with block displacements and rotations: $\mathbf{d}^{panel} = \mathbf{H}^{panel}\mathbf{q}^{panel}$. Then, panel stiffness matrix may be calculated as: $\mathbf{K}^{panel} = (\mathbf{H}^{panel})^T \bar{\mathbf{K}}^{panel} \mathbf{H}^{panel}$, where $\bar{\mathbf{K}}^{panel}$ is a diagonal matrix collecting interface stiffness values of the entire panel.

2.1 Yield criterion for interface

In this work, the nonlinear behaviour of interfaces is assumed to be governed by a simple Mohr-Coulomb yield criterion, characterized by a cohesion c and a friction ratio $\mu = \tan\varphi$:

$$|\sigma_s| \leq c - \sigma_n \tan\varphi, \tag{7}$$

where σ_s ia a generic shear stress over the interface with a generic plane direction ($\sigma_s = \sqrt{\sigma_{s,1}^2 + \sigma_{s,2}^2}$) and negative values of normal stress σ_n are assumed in case of compression. Moreover, normal stresses must be less than interface tensile strength $\bar{\sigma}_t$, if present:

$$\sigma_n \leq \bar{\sigma}_t. \tag{8}$$

For instance, dry interfaces cannot support tension and have a negligible cohesion, whereas mortar joints are characterized by a tensile strength $\bar{\sigma}_t$ that may be determined by means of experimental tests (EN 1015-11:2007). Tensile strength value may become a cap for the graph represented by Equation (7) or, for simplicity, it may be assumed equal to the normal stress corresponding to a null shear strength: $\bar{\sigma}_t = c / \tan\varphi$. Mortar joints cohesion may be determined by means of experimental tests (EN 1052-3:2002). In any case, both dry or mortar interface types are characterized by a frictional behaviour and an unlimited compressive strength is assumed.

Considering a generic horizontal or vertical interface (Figure 2a,b) and assuming a local coordinate system $y_1y_2y_3$, with plane y_1y_2 coincident with interface mid-plane and y_3 orthogonal to it, forces and moments exerted by two adjacent blocks at the interface centre are: normal force $f_3\mathbf{e}_3 = f_n\mathbf{e}_3$, shear forces $f_1\mathbf{e}_1$, $f_2\mathbf{e}_2$, bending moments $m_1\mathbf{e}_1, m_2\mathbf{e}_2$ and torsion $m_3\mathbf{e}_3$ (Figure 2c).

In order to obtain an interface yield criterion based on Equations (7-8) but related to interface actions, a simple interface model is introduced and interface area is subdivided in rectangular portions and a set of springs acting on each sub-element centre is defined (Figure 3a,b). Each spring is characterized by a normal and a shear stiffness (k_n and k_s) and Mohr-Coulomb yield criterion and no-tension criterion are adopted for restraining normal and shear forces transmitted by each spring. In case of mortar joints, k_n and k_s depend on mortar elastic modulus and Poisson ratio (E^m, ν^m), and joint thickness e: $k_n = E^m / e$, $k_n = E^m / [2(1+\nu^m)] = G^m / e$; whereas in case of dry joints, normal stiffness value may be set equal to a large fictitious value in order to avoid compenetration between adjacent blocks. The main purpose of this model is to assess numerically interface behaviour and its strength by discretising the distributions of normal and shear stresses acting on the interface considered.

It may be pointed out that the proposed interface model turns on to be coincident with the problem of a rigid 3D indenter on a Winkler elastic-plastic support with friction; in particular, the forces of each spring do not depend on the deformation of other springs and the displacement of the rigid indenter is represented by the relative displacement between the adjacent blocks connected by the interface. Moreover, modelling an interface element by means of a discretization of its cross-section is an approach quite close to that adopted in fiber beam finite elements (Spacone et al., 1996), then a possible further development of the proposed DEM may be related to the adoption of fibre beam FEs for representing the nonlinear behaviour of interfaces, in particular in case of mortar interfaces connecting rigid blocks.

In the following sub-paragraphs, the effects of shear forces, torsion and bending moments over an interface are evaluated by means of the spring model described above. The dry interface between two rigid blocks studied by Orduña (2004) is here considered (Figure 3b). Block dimensions are: width b = 0.3 m, height a = 0.2 and thickness s = 0.2 m, whereas block volumetric weight is γ = 20 kN/m^3, leading to a compressive force over the interface equal to 240 N. Interface stiffness values are k_n = 2.4 MPa/mm and k_s = 1 MPa/mm and friction ratio is μ = 0.7. Interface dimensions are equal to block width and thickness ($l_1 = b$ and $l_2 = s$) and in order to obtain sufficiently accurate solutions, interface sides are subdivided in 32 portions, leading to a set of 1024 springs equally spaced in both plane directions.

2.1.1 Normal and flexural yield criterion

Considering for first interface normal force and bending moments, the yield criterion is governed by tensile strength, if present, whereas unlimited compressive strength is considered. Normal force and bending moments must not generate tensile stresses larger than the corresponding strength, hence they must satisfy the following conditions:

$$\begin{aligned} & f_n = f_3 \leq f_t, \\ & |m_1| \leq (f_t - f_n)\, l_{c1}, \\ & |m_2| \leq (f_t - f_n)\, l_{c2}. \end{aligned} \tag{9}$$

Where $f_t = \bar{\sigma}_t\, S$ represents the tensile strength of the entire interface, defined as the product of tensile strength $\bar{\sigma}_t$ and interface area (S_v or S_h). Distance l_{ci} with i = 1,2 is the characteristic length of the interface with respect to interface plane directions, namely the maximum eccentricity of normal force with respect to block centre that may be supported by the interface. Each value is equal to $l_{c1} = s/2, l_{c2} = b/4$ for a horizontal interface and to $l_{c1} = a/2, l_{c2} = s/2$ for a vertical one. First and second conditions in Equation (9) have been already adopted by authors for the in plane case (Baraldi and Cecchi, 2016a) and they turn out to be coincident to those adopted by Trovalusci and Masiani (2003). In particular, the first condition may be defined as 'detachment' condition, whereas the second and third ones may be defined as 'rotation' conditions with respect to y_1 and y_2 axis. It is worth noting that the actual stress distributions given by normal forces and bending moments are not taken into account for simplicity, following the hypothesis adopted by Orduña and Lourenco (2005a). In particular, uniform normal stress distributions are considered, also in case of increasing bending moments and if the combination of normal force and bending moments do not respect the middle-third rule, uniform stresses over reduced rectangular areas are considered.

2.1.2 Shear yield criterion

In this subparagraph interface shear strength is studied by adopting the simple spring model based on interface subdivision and elastic-perfectly plastic frictional springs. The interface subject to shear in both plane directions is studied and a compressive force given by the self-weight of the block over the interface f_3 = -240 N is considered. Several incremental analyses are performed by applying to the model a set of relative shear displacements with varying direction on y_1y_2 plane (Figure 4), in order to obtain interface shear strength along each plane direction and to evaluate the effect of combined shear forces along plane directions.

Considering the model adopted for studying interface behaviour, each spring is compressed by a portion of block self-weight and it is subject to the same overall relative shear displacement of the interface; then each spring is subject to the same normal and shear force. This conditions represents the uniform distribution of normal and shear stresses over the original entire interface; moreover it must be pointed out that in this case the number of subdivisions of interface area does not affect results.

Figure 5 shows for first the shear force-relative displacement incremental curves in y_1 and y_2 directions and then it presents the strength domain for combined shear forces. In this case shear strength depends only on friction ratio and on the applied normal force, then the corresponding value along a generic plane direction is equal to $f_{s,u} = -\mu f_3 = 168\ \text{N}$. Such value is reached by analyses characterized by relative displacements along one plane direction only and also by analyses with relative displacements in both plane directions. The resulting strength domain is represented by a circle, characterized by the expression $f_1^2 + f_2^2 \le f_{s,u}^2 = (-\mu f_3)^2$. More generally, considering also the effect of joint cohesion or tensile strength $f_t = \bar{\sigma}_t S$, the interface shear strength domain is defined by the well-known Mohr-Coulomb yield criterion in terms of shear force resultants:

$$f_1^2 + f_2^2 \le [\mu (f_t - f_n)]^2 \tag{10}$$

That may be written also as $(f_1^2 + f_2^2) / f_{s,u}^2 \le 1$. Such relationship is adopted in the following numerical tests without any approximation of the domain, whereas several authors are used to simplify the circular domain with a polygonal (octagonal) shape (Orduña and Lourenco, 2005a).

2.1.3 Torsion yield criterion

Considering the simple spring model, torsion strength is evaluated for first in case of pure torsion, hence a relative rotation δ_3 is applied to the blocks connected by the interface (Figure 6a). A torsion strength $m_{3,u} = 16.2\ \text{Nm}$ is obtained, this value turns out to depend on friction ratio and compressive force by means of a torsion constant: $m_{3,u} = c_T(-\mu f_3)$. With

$$c_T = \frac{1}{3}\left[\frac{c}{2} + \frac{l_1^2}{2l_2^2}\ln\left(\frac{l_2 + c}{l_1}\right) + \frac{l_2^2}{2l_1^2}\ln\left(\frac{l_1 + c}{l_2}\right)\right] \tag{11}$$

where $c = \sqrt{l_1^2 + l_2^2}$. Such constant may be obtained analytically by solving the integral of shear stresses generated by a plastic torsion of the interface and the corresponding expression may be found in the original work of Orduña (2004) or in a recent work of Portioli et al. (2013). If interface cohesion is present or interface tensile strength f_t is not negligible, torsion strength increases in the same way of shear strength and the yield criterion in case of pure torsion is given by:

$$| m_3 | \leq c_T [\mu (f_t - f_n)] \quad \text{if} \quad f_1^2 + f_2^2 = 0 . \tag{12}$$

Appendix collects more details obtained by performing numerical analyses with the proposed spring model with varying cohesion values.

In case of pure torsion, the twisting centre coincides with interface centre and Figure 7a shows the corresponding shear stress lines. If a combination of shear force and torsion is considered, the twisting centre moves towards to interface centre, as showed in Figure 7b and in appendix by Figure A2. Such shear stress lines are found performing several incremental analyses characterized by a relative rotation δ_3 and a relative displacement d_1 (Figure 6b). Moreover in appendix, further images related to the case of combined torsion and shear in both plane directions are presented. As can be expected, the torsion strength is strictly related with the shear strength and vice-versa if combined actions are present; in particular, torsion strength decreases for increasing the applied shear force and similarly shear strength decreases for increasing the applied torsion. Figure 8 shows shear-relative displacement and torsion-relative rotation curves of several incremental analyses performed with the adopted spring model; then, ultimate values of torsion and shear force are combined into a m_3-f_1 strength domain. In order to appreciate the shape of such domain, the circular curve $(m_3 / m_{3,u})^2 + (f_1 / f_{s,u})^2 = 1$ is plotted over the domain with a dashed line, showing that the actual m_3-f_1 strength domain does not have a perfect circular shape. Following the analytic results showed by Orduña and Lourenco (2005a), the shape of torsion-shear strength domain depends on the ratio between interface width and depth l_1/l_2, and in order to avoid such effect, they adopted a simplified polygonal domain, as they did in case of combined plane shear actions. Figure 9 shows dimensionless m_3-f_1 strength domains obtained with the proposed spring model for varying l_1/l_2. In appendix, each domain is presented separately from the others and a proposal of a unique expression of strength domain accounting also for l_1/l_2 is proposed.

Finally, the effect of bending moments m_1, m_2 (acting separated and combined) on torsion strength is investigated with the proposed spring model. Following the considerations of Orduña and Lourenco (2005a), in case of negligible tensile strength, the interface cannot tolerate tensile actions, then the effective area subject to compression is reduced to a smaller rectangle accounting for the eccentricity in both plane directions given by bending moments. As previously stated, the simplification done by Orduña and Lourenco (2005a) is based on hypothesis of uniform compressive stresses over the reduced rectangular area. The same hypothesis was taken into account recently by Casapulla and Portioli (2015). Adopting the same hypothesis with the proposed spring model, the interaction between bending moments and torsion strength is evaluated for the interface assumed as reference. Incremental analyses are then performed by applying an increasing relative rotation over a reduced rectangular area due to applied bending moments. Figure 10 shows torsion strength obtained numerically as function of m_1 and m_2; the domain turns out to be in excellent agreement with the one obtained analytically by Orduña and Lourenco (2005a).

2.2 Nonlinear interface behaviour

In general, considering each force and couple acting over a generic interface (Figure 2c), a simple elastic-perfectly plastic relation between actions and relative displacements is adopted. Hence, after having defined interface strength detailed for each component of the actions that may be transmitted by adjacent blocks in a 3D problem, each interface strength is assumed as the elastic limit of the elastic-perfectly plastic action-relative displacement curve. Then, the relationship between interface normal force and relative normal displacement and the relationships between interface bending moments and relative rotations follow an elastic-perfectly plastic behaviour. Moreover, an interaction between different failure modes is introduced. For instance, if the interface is subject to excessive plane rotation, only its rotational stiffness is set equal to zero, whereas if the interface is subject to detachment, all interface stiffness values are set equal to zero:

$$\begin{aligned} &f_n > f_t \rightarrow k_n = k_t = k_r = 0, \\ &|m_i| > (f_t - f_n) l_{ci} \rightarrow k_r = 0 \quad i = 1, 2. \end{aligned} \tag{13}$$

An elastic-plastic behaviour is assumed if restraint conditions for shear force and torsion are not respected. In particular, interface tangential stiffness k_t is set equal to zero, whereas normal and flexural stiffness values are not modified.

$$f_1^2 + f_2^2 > [\mu (f_t - f_n)]^2 \rightarrow k_t = 0,$$
$$(m_3 / m_{3,u})^{\alpha} + (f_1^2 + f_2^2) / [\mu (f_t - f_n)]^2 > 1 \rightarrow k_t = 0. \quad (14)$$

Where $m_{3,u} = c_T \mu (f_t - f_n)$ if bending moments are not present, otherwise $m_{3,u}$ is reduced due to bending moment effects as showed by Figure 10. Exponent α in the above equation may be assumed equal to 1.43 in case of interface dimension ratio l_1/l_2 close to 1 or α equal to 1.50 considering typical interfaces in masonry panels with regular texture and standardized bricks. Further details may be found in appendix.

2.3 Nonlinear DEM

Restraint conditions for interface forces and moments allow to define the elastic limits of force-relative displacement and moment-relative rotation constitutive laws, that are assumed to be elastic-perfectly plastic. Then, incremental analyses or pushover analyses may be performed by applying incremental loads to the discrete model and updating the stiffness matrix $\mathbf{K}^{panel}$ accounting for local interface nonlinear behaviour. For instance, the stiffness matrix at a generic load step i is based on interface damage at the previous step i-1. A generic incremental analysis may be performed by applying several load steps and evaluating for first the corresponding displacement increments $\delta\mathbf{q}_i$ and then the internal forces $\mathbf{F}_i^{int}$ transmitted along interfaces: $\delta\mathbf{q}_i = (\mathbf{K}^{panel}{}_{(\mathbf{q}_{i-1})})^{-1}\delta\mathbf{F}^{ext}$, $\mathbf{F}_i^{int} = \mathbf{F}_{i-1}^{int} + \mathbf{K}^{panel}{}_{(\mathbf{q}_{i-1})}\delta\mathbf{q}_i$.

Internal forces are corrected accounting for the yield criterion adopted, then residual forces with respect to applied loads $\mathbf{F}^{ext}$ may be obtained: $\mathbf{R}_i = \mathbf{F}_i^{int} - \mathbf{F}^{ext}$. Then, a typical iterative process is performed in order to reduce residual forces less than a predefined tolerance. Similarly to the case limited to in plane actions and displacements, the proposed DEM allows to study regular block assemblages by adopting traditional procedures commonly used in nonlinear FE analysis.

In the following paragraphs, numerical tests are performed considering masonry panels subject to self-weight and increasing lateral loads. Such loads are proportional to the weight ($P = \gamma\, a\, b\, s$, where γ is block volumetric weight) and are identified by the load multiplier λ; then, the vector collecting the total forces applied at block centres may be defined as $\mathbf{F}^{ext} = \mathbf{F}_D + \lambda\mathbf{F}_L$, where $\mathbf{F}_D$ collects dead loads represented by block self-weight P and further vertical loads and $\lambda\mathbf{F}_L$ represents unknown horizontal live loads (in or out of plane).

3 OUT OF PLANE NUMERICAL EXPERIMENTS

The proposed discrete model is able to represent the behaviour of masonry panels with regular texture characterized by dry joints or weak mortar joints. Analyses of specimens subject to self-weight and increasing in plane lateral loads have been already performed by authors by adopting a model limited to in plane DOFs (Baraldi and Cecchi, 2016a) and recently these analyses have been carried out also with the full 3D model proposed here (Baraldi and Cecchi, 2016b) showing coincident results, as expected, and in good agreement with other numerical solutions and laboratory tests.

Then in this paragraph, several numerical experiments are carried on in order to evaluate the effectiveness of the proposed nonlinear DEM in the determination of out of plane collapse mechanisms and limit loads of masonry panels. It is worth noting that nonlinear out of plane behaviour is strictly dependent on in plane actions such as dead loads, hence in this case out of plane degrees of freedom cannot be considered uncoupled by in plane degrees of freedom.

Talking about out of plane behaviour of masonry, the typical mechanisms described by Rondelet (1802) may be taken into account. Numerical experiments in first and second subparagraphs of this section are going to reproduce numerically the typical out of plane mechanisms of masonry panels with dry joints, taking as reference several existing results, both numerical and experimental. In particular, the first mechanism type defined by Rondelet is the typical out of plane rigid rotation of a free masonry wall with respect to its base (Figure 11a), whereas the second mechanism regards a masonry wall restrained along a vertical edge by an orthogonal wall, leading to the development of a diagonal crack and to a rotation of a triangular wall portion (Figure 11b). This mechanism is characterized by a larger ultimate load with respect to the previous case due to the lateral restraint. The third mechanism regards a masonry wall restrained by two orthogonal walls at both vertical edges; in this case a vertical crack along panel axis of symmetry develops together with two diagonal cracks starting from panel upper corners (Figure 11c), leading to two triangular wall portions that rotate with respect to diagonal cracks. In this last case, the ultimate load is larger than those of the previous mechanisms due to the lateral restraints.

In the second subparagraph of this section, further numerical examples are dedicated to masonry panels with dry joints loaded by wooden beams and masonry panels with openings. Finally in the third subparagraph of this section, masonry panels with mortar joints are considered and laboratory tests of panels supported along three and four sides are reproduced. Restraints along three sides lead to a collapse mechanism coincident with the third one

proposed by Rondelet (Figure 11c), whereas restraints along four sides lead to a collapse mechanism with four diagonal cracks (Figure 11d).

3.1 Case studies proposed by Orduña and Lourenço

Two simple examples of masonry panels out of plane loaded are taken into account for first by assuming as reference the numerical tests performed by Orduña and Lourenço (2005b). In both cases masonry panels are made of blocks with running bond arrangement and having dimensions a = 0.081 m, b = 0.210 m, s = 0.07 m and volumetric weight equal to 20 kN/m^3. Contacts between blocks are dry, with μ = 0.7 and null cohesion and tensile strength. In the first example, panel dimensions are: length L = 0.630 m, height H = 1.053 m and thickness s = 0.07 m, obtained by assembling 3 blocks along panel length and 13 blocks along its height; block translations are fixed along panel left column (Figure 12a). In the second example panel dimensions are: L = 1.260 m, H = 1.053 m and s = 0.07 m, obtained with 6 blocks along panel length and 13 blocks along its height; block translations are fixed along both lateral columns (Figure 12b).

Figure 13a shows a collapse mechanism characterized by a diagonal crack starting from the right side of the panel after the 2nd row of blocks. Such mechanism is in quite good agreement with the one showed in the original analysis and the limit load obtained with the proposed nonlinear DEM is included between FEM and limit analysis performed by Orduña and Lourenço (Table 1). Figure 13b shows a collapse mechanism characterized by a symmetric flexural deformation with large displacements along vertical axis of symmetry. Similarly to the previous case, collapse mechanism and limit load (Table 1) are in quite good agreement with reference solutions.

3.2 Restrepo Vélez, Magenes and Griffith experiments

In this paragraph, several experimental tests performed by Restrepo Vélez et al. (2014) are taken as reference. Original tests were performed on scaled masonry-like specimens with dry joints, subject to self-weight and increasing out of plane loads by means of an inclined plane machine, in order to obtain out of plane failure mechanisms. Block dimensions are a = 28.24 mm, b = 79.78 mm and s = 39.68 mm and block volumetric weight is 26.8 kN/m^3. Dry joints are characterized by friction ratio μ = 0.7, with null cohesion and null tensile strength. All cases are characterized by 21 block courses along panel height and varying number n of blocks along panel length (from 4 to 14, for instance). Panel restraints at one or both lateral

edges are obtained with one or two orthogonal walls (Figure 14a and b, respectively); for this reason, several mechanisms turned out to involve also blocks in orthogonal walls. In the following numerical experiments, the effect of orthogonal walls is simply modelled by restraining block translations and rotations along one or both lateral columns (Figure 14e and f, respectively). Then, the present model will not be able to represent complex collapse mechanisms involving orthogonal walls, leading to small differences between proposed numerical results and experimental tests. Moreover, additional specimen types considered a panel without orthogonal walls simply supported at the base and loaded by several wooden beams (Figure 14c) and panels with openings (Figure 14d).

Figure 15 shows failure mechanisms of several panels restrained along left column, varying the number of blocks along panel length (for further details about block number see the first row of Table 2). Mechanisms are characterized by a diagonal crack starting from lower-right panel corner, directed towards the upper-left panel corner and a triangular/trapezoidal portion of panel is subject to an out of plane roto-translation with respect to such diagonal crack. These mechanism types are in quite good agreement with experimental tests, moreover numerical results obtained with the proposed nonlinear DEM are in quite good agreement with experimental results (Table 2), especially for specimens S11, S12 and S13, thanks to the large number of blocks of the models, whereas for specimen S15, characterized by a small number of blocks along panel length, limit load obtained with DEM is quite far from experimental result with respect to other cases. Figure 16 shows failure mechanisms of several panels restrained along both lateral vertical edges. Such mechanisms are characterized by a vertical crack along the axis of symmetry of the panel and diagonal cracks starting from lateral edges and moving down to panel axis of symmetry. Mechanisms are similar but not coincident with respect to those obtained experimentally, due to the actual restraint adopted for masonry specimens; however limit loads obtained numerically with nonlinear DEM are still in quite good agreement with experimental results. Figure 17 shows the failure mechanism of a simply supported panel loaded by eleven wooden beams (16.46 N transmitted by each beam) and subject to increasing out of plane loads (see Figure 14c for the corresponding specimen type and Figure 14g for the corresponding DEM representation). The mechanism is characterized by a horizontal hinge in the upper portion of the panel, along the joints between the 15^{th} and 16^{th} block courses and it is almost coincident with the real mechanism obtained during laboratory tests; similarly, the collapse load is close to the one evaluated experimentally. Finally Figure 18 show the failure mechanisms of two masonry

walls with openings, the first one with a wide central pier (specimen S23) and the second one with a thin central pier (specimen S24). In both cases, collapse obtained with the proposed DEM is characterized by the out of plane rotation of the central pier and the connected spandrels over the openings, with diagonal cracks starting from the opening bottom to the midpoint of panel base. Such mechanisms are not completely coincident with those obtained in laboratory that were characterized by an evident out of plane flexural deformation of the entire upper portion of the wall, involving also the upper portion of the orthogonal walls. Similarly to previous cases, such differences are caused by the not completely correct representation of lateral restraints. Limit loads obtained with the proposed DEM, however, are in quite good agreement with those obtained experimentally (Table 2).

3.3 Chee Liang experiments

Finally in this subparagraph, analyses on masonry panels with mortar joints are performed. The experimental campaign carried out by Chee Liang (1996) is considered and several specimens are taken as reference and studied with the proposed DEM model. It is worth noting that such specimens are frequently taken as reference by researchers involved in the formulation of models and methods for the collapse analysis of out of plane loaded masonry walls ((Macorini and Izzuddin, 2011; Milani and Taliercio, 2016).

Masonry specimens tested by Chee Liang have square or rectangular shape, they are made of clay bricks in running bond pattern and they are simply supported along four sides or three sides (Figure 19). During all experiments masonry specimens are subject to self-weight and to an increasing uniform out of plane pressure p. Block dimensions are b = 0.112 m, a = 0.036 m, s = 0.053 m and mortar joint thickness is e = 0.01 m. Mortar interface stiffness values are assumed equal to those adopted by Liang for simulating experimental tests with a FE model, in particular k_n = 25. N/mm^3 and k_t = 105 N/mm^3 (Macorini and Izzuddin, 2011). Interface friction ratio is μ = 0.57 and tensile strength is $\bar{\sigma}_t = 0.35$ MPa . Among the specimens tested by Chee Liang, the following numerical tests regard three of them characterized by simple supports along the four sides, two of them with three supported sides and free top side and the last test is characterized by three supported sides and free left side. Specimen dimensions and restraint case are listed in Table 3, together with ultimate out of plane pressure p obtained with the proposed nonlinear DEM and with laboratory tests. Numerical results are in quite good agreement with laboratory tests, whereas the final damaged configurations obtained numerically, showed in Figures 20-21 are a bit different than laboratory results, due to the

perfect symmetry of discrete models and applied loads that generate symmetric displacements and symmetric interface damage. Masonry specimens supported along four sides are characterized by diagonal cracks from panel corners to panel centre, following the generic mechanism already presented in Figure 11d, whereas masonry specimens supported along three sides are characterized by two diagonal cracks starting from the restrained corners and a straight crack along panel axis of symmetry starting from the midpoint of the free edge. Further information that may be obtained with the proposed model are the load-displacement curves related to each analysis (Figure 22), collecting out of plane displacement evaluated at each panel centre in case of panels with four side simply supported or at the midpoint of the free side in the other cases considered. The proposed DEM is able to predict the ultimate loads obtained experimentally but the models are stiffer than the real specimens, probably due to the rigid block hypothesis adopted; in fact DEM out of plane displacements turn out to be smaller than those obtained experimentally.

4 CONCLUSIONS

In this work, the 3D DEM introduced by Cecchi and Sab (2004) for modelling regular masonry in the linear elastic field has been extended to the collapse analysis of masonry panels with dry and mortar joints by adopting a Mohr-Coulomb yield criterion for defining elastic limits to interface actions. A simplified elastic-perfectly plastic spring model has been adopted for studying the local behaviour of a generic interface subject to independent and combined normal, shear, bending and torsion actions. The spring model allowed to discretize normal and shear interface stresses, in order to obtain simple expressions of interface strength in terms of force and moment resultants, that turned out to be coincident with those obtained analytically by Orduña and Lourenço (2005a), but without the necessity of introducing simplified strength domains in case of combined shear forces and combined shear force with torsion.

The proposed nonlinear 3D DEM allowed to perform incremental analyses of several masonry specimens by adopting the traditional procedures used for nonlinear FE analysis, with a small computational effort due to the small number of DOFs involved. The model turned out to be simple and effective in the determination of limit loads and collapse mechanisms of masonry panels having regular texture, with dry and mortar joints, subject to self-weight and out of plane loads.

Several numerical tests reproduced the laboratory campaign carried out by Restrepo Vélez et al. (2014) on masonry specimens with dry joints, in this case the nonlinear DEM simulated correctly limit loads of the specimens taken into account. Moreover, considering collapse mechanisms, the ones relative to panels restrained by a lateral orthogonal wall have been reproduced correctly by the DEM, whereas small differences have been found in collapse mechanisms relative to panels restrained by orthogonal walls along panel lateral edges. Further numerical tests reproduced the laboratory campaign carried out by Chee Liang (1996) with masonry specimens with mortar joints. Similarly to previous cases, the nonlinear DEM simulated correctly limit lateral pressures, even if the corresponding collapse mechanisms turned out to be obviously perfectly symmetric with small differences with respect to the observed damage patterns. Moreover, the nonlinear DEM allowed to obtain load-displacement incremental curves as further information on the collapse behaviour of the specimens considered.

Further developments of the model will regard the assessment of nonlinear analysis of more complex masonry specimens, characterized for example by blocks arranged irregularly and real 3D structures with orthogonal walls and roofs.

REFERENCES

Baggio, C., Trovalusci, P., 1993. Discrete models for jointed block masonry walls. The Sixth North American Masonry Conference, Philadelphia, Pennsylvania, June 6-9.

Baggio, C., Trovalusci, P., 1998. Limit analysis for no-tension and frictional three-dimensional discrete systems. Mech. Struct. Mach., 26 (3), 287-304. DOI: 10.1080/08905459708945496

Baraldi, D., Cecchi, A., Tralli, A., 2015. Discrete and Continuous Models for Out-of-Plane Loaded Masonry Like Structures: A Multiscale Comparative Study. J. Kruis, Y. Tsompanakis, B.H.V. Topping, (Editors), Proceedings of the Fifteenth International Conference on Civil, Structural and Environmental Engineering Computing, Civil-Comp Press, Stirlingshire, UK, Paper 207, Prague, Czech Republic, September 1-4.

Baraldi, D., Cecchi, A., 2016a. Discrete approaches for the nonlinear analysis of in plane loaded masonry walls: Molecular dynamic and static algorithm solutions. Eur. J. Mech. A/Solids, 57, 165-177. DOI: 10.1016/j.euromechsol.2015.12.008

Baraldi, D., Cecchi, A., 2016b. Three-dimensional nonlinear behaviour of masonry walls modelled with discrete elements. ECCOMAS Congress 2016 VII European Congress on Computational Methods in Applied Sciences and Engineering. M. Papadrakakis, V. Papadopoulos, G. Stefanou, V. Plevris (eds.), Crete Island, Greece, 5–10 June 2016.

Baraldi, D., Cecchi, A., 2016c. Discrete and Continuous Models for Static and Modal Analysis of Out of Plane Loaded Masonry. Submitted to Computer & Structures.

Baraldi, D., Bullo, S., Cecchi, A., 2016. Continuous and discrete strategies for the modal analysis of regular masonry. Int. J. Solids Struct., 84, 82-98. DOI: 10.1016/j.ijsolstr.2016.01.015

Casapulla, C., Portioli, F., 2015. Experimental and analytical investigation on the frictional contact behavior of 3D masonry block assemblages. Constr. Building Mater., 78, 126-143. DOI: 10.1016/j.conbuildmat.2014.12.100

Casapulla, C., Portioli, F., 2016. Experimental tests on the limit states of dry-jointed tuff blocks. Mater. Struct., 49, 751–767. DOI: 10.1617/s11527-015-0536-3

Casolo, S., 2000. Modelling the out-of-plane seismic behaviour of masonry walls by rigid elements. Earthq. Eng. Struct. Dyn., 29, 1797-1813. DOI: 10.1002/1096-9845(200012)29:12<1797::AID-EQE987>3.0.CO;2-D

Cecchi, A., Sab, K., 2004. A comparison between a 3D discrete model and two homogenised plate models for periodic elastic brickwork. Int. J. Solids Struct., 41 (9-10), 2259-2276. DOI: 10.1016/j.ijsolstr.2003.12.020

Chee Liang, N.G., 1996. Experimental and theoretical investigation of the behaviour of brickwork cladding panel subjected to lateral loading. Ph.D. thesis.

D'Ayala, D., Speranza, E., 2003. Definition of collapse mechanisms and seismic vulnerability of masonry structures. Earthq. Spectra, 19 (3), 479-509. DOI: http://dx.doi.org/10.1193/1.1599896

de Felice, G., Giannini, R., 2001. Out of plane seismic resistance of masonry walls. Journal of Earthq. Eng., 5 (2), 253-271. DOI: 10.1080/13632460109350394

EN 1015-11:2007, Methods of test for mortar for masonry. Part 11: determination of flexural and compressive strength of hardened mortar.

EN 1052-3:2002, Methods of test for masonry. Part 3: Determination of initial shear strength.

Ferreira, T.M., Costa, A.A, Costa, A., 2015. Analysis of the Out-Of-Plane Seismic Behavior of Unreinforced Masonry: A Literature Review. Int. J. Archit. Herit., 9 (8), 949-972. DOI: 10.1080/15583058.2014.885996

Ferris, M.C., Tin-Loi, F., 2001. Limit analysis of frictional block assemblies as a mathematical program with complementarity constraints. Int. J. Mech. Sci., 43, 209-224. DOI: 10.1016/S0020-7403(99)00111-3

Gilbert, M., Melbourne, C., 1994. Rigid block analysis of masonry structures. Struct. Eng., 72(21), 356-361.

Giuffrè, A., 1991. Letture sulla meccanica delle murature storiche, Edizioni Kappa: Roma (in Italian).

Griffith, M.C., Lam, N.T.K., Wilson J.L., Doherty, K., 2004. Experimental investigation of unreinforced brick masonry walls in flexure. J. Struct. Eng., 130(3), 423-431. DOI: 10.1061/(ASCE)0733-9445(2004)130:3(423)

Livesley R.K., 1978. Limit analysis of structures formed from rigid blocks. Int. J. Numer. Methods Eng., 12, 1853-1871. DOI: 10.1002/nme.1620121207

Livesley R.K., 1992. A computational model for the limit analysis of three-dimensional masonry structures. Meccanica, 27, 161-172. DOI: 10.1007/BF00430042

Macorini, L., Izzuddin, B.A., 2011. A non-linear interface element for 3D mesoscale analysis of brick-masonry structures. Int. J. Numer. Methods Eng., 85, 1584-1608. DOI: 10.1002/nme.3046

Milani, G., Zuccarello, F.A., Olivito, R.S., Tralli, A., 2007. Heterogeneous upper-bound finite element limit analysis of masonry walls out-of-plane loaded. Comput. Mech., 40(6), 911-931. DOI: 10.1007/s00466-006-0151-9

Milani, G., Taliercio, A., 2016. Limit analysis of transversally loaded masonry walls using an innovative macroscopic strength criterion. Int. J. Solids Struct., 81, 274-293. DOI: 10.1016/j.ijsolstr.2015.12.004

Orduña Bustamante, A., 2003. Seismic Assessment of Ancient Masonry Structures by Rigid Blocks Limit Analysis, Ph.D. thesis.

Orduña, A., Lourenço, P.B., 2005a. Three-dimensional limit analysis of rigid blocks assemblages. Part I: Torsion failure on frictional interfaces and limit analysis formulation. Int. J. Solids Struct., 42 (18-19), 5140-5160. DOI: 10.1016/j.ijsolstr.2005.02.010

Orduña, A., Lourenço, P.B., 2005b. Three-dimensional limit analysis of rigid blocks assemblages. Part II: Load-path following solution procedure and validation. Int. J. Solids Struct., 42 (18-19), 5161-5180. DOI: 10.1016/j.ijsolstr.2005.02.011

Portioli, F., Casapulla, C., Cascini, L., D'Aniello, M., Landolfo, R., 2013. Limit analysis by linear programming of 3D masonry structures with associative friction laws and torsion interaction effects. Arch. Appl. Mech., 83, 1415-1438. DOI: 10.1007/s00419-013-0755-4

Restrepo Vélez, L.F., Magenes, G., Griffith, M.C., 2014. Dry stone masonry walls in bending – Part I: static tests, Int. J. Archit. Herit., 8, 1-28. DOI: 10.1080/15583058.2012.663059

Rondelet, J.B., 1802. Traité théorique et pratique de l'art de bâtir. Paris, France.

Smoljanović, H., Živaljić, N., Nikolić, Ž., 2013. Overview of the methods for the modeling of historical masonry structures. Gradevinar, 65 (7), 607-618.

Stefanou, I., Sulem, J., Vardoulakis, I., 2008. Three-dimensional Cosserat homogenization of masonry structures: elasticity. Acta Geotechnica, 3, 71-83. DOI: 10.1007/s11440-007-0051-y

Spacone, E., Filippou, F.C., Taucer, F., 1996. Fibre beam–column model for non-linear analysis of r/c frames: part i. Formulation. Earthq. Eng. Struct. Dyn., 27 (7), 711-725. DOI: 10.1002/(SICI)1096-9845(199607)25:7<711::AID-EQE576>3.0.CO;2-9

Trovalusci, P., Masiani, R., 2003. Non-linear micropolar and classical continua for anisotropic discontinuous materials. Int. J. Solids Struct., 40, 1281-1297. DOI:10.1016/S0020-7683(02)00584-X

van der Pluijm, R., 1999. Out-of-Plane Bending of Masonry Behaviour and Strength. Ph. D. Thesis.

West, H.W.H., Hodgkinson, H.R., Haseltine, H.A., 1977. The Resistance of Brickwork to Lateral Loading. Part 1 Experimental Methods and Results of Tests on Small Specimens and Full Sized Walls. Struct. Eng., 55(10), 411-421.

Appendix

Compatibility matrix

As stated in paragraph 2, relative translations and rotations between two adjacent blocks connected by a generic interface may be related to global block translations and rotations (or Lagrangian parameters). Equations (3) may be re-written in case of two generic adjacent blocks by introducing the generic in plane distances dy_1, dy_2 between the corresponding centres:

$$\begin{aligned}
d_1^{k_1,k_2} &= u_1^{i+k_1,j+k_2} - u_1^{i,j} + dy_2(\omega_3^{i+k_1,j+k_2} + \omega_3^{i,j})/2, \\
d_2^{k_1,k_2} &= u_2^{i+k_1,j+k_2} - u_2^{i,j} - dy_1(\omega_3^{i+k_1,j+k_2} + \omega_3^{i,j})/2, \\
d_3^{k_1,k_2} &= u_3^{i+k_1,j+k_2} - u_3^{i,j} + dy_1(\omega_2^{i+k_1,j+k_2} + \omega_2^{i,j})/2 - dy_2(\omega_1^{i+k_1,j+k_2} + \omega_1^{i,j})/2, \\
\delta_1^{k_1,k_2} &= \omega_1^{i+k_1,j+k_2} - \omega_1^{i,j}, \\
\delta_2^{k_1,k_2} &= \omega_2^{i+k_1,j+k_2} - \omega_2^{i,j}, \\
\delta_3^{k_1,k_2} &= \omega_3^{i+k_1,j+k_2} - \omega_3^{i,j}.
\end{aligned} \tag{A1}$$

Then, the 'compatibility' matrix at interface level $\mathbf{H}^{k_1,k_2}$, needed for relating interface relative displacements with global block displacements ($\mathbf{d}^{k_1,k_2} = \mathbf{H}^{k_1,k_2}\mathbf{q}^{k_1,k_2}$), is a 6-by-12 matrix obtained by assembling several sub-matrices as follows:

$$\mathbf{H}^{k_1,k_2} = \begin{bmatrix} -\mathbf{I} & -\mathbf{D}_i & \mathbf{I} & \mathbf{D}_j \\ \mathbf{0} & -\mathbf{I} & \mathbf{0} & \mathbf{I} \end{bmatrix}, \tag{A2}$$

where **I** and **0** are, respectively, identical and zeros 3-by-3 matrices and

$$\mathbf{D}_i = \frac{1}{2}\begin{bmatrix} 0 & 0 & -dy_2 \\ 0 & 0 & dy_1 \\ dy_2 & -dy_1 & 0 \end{bmatrix}, \quad \mathbf{D}_j = \frac{1}{2}\begin{bmatrix} 0 & 0 & dy_2 \\ 0 & 0 & -dy_1 \\ -dy_2 & dy_1 & 0 \end{bmatrix}. \tag{A3}$$

Torsion strength

In this subparagraph, further details about numerical tests performed with the proposed spring model for determining interface torsion strength and the effects of tensile strength and combined shear forces on torsion strength are presented.

For first, the effect of interface tensile strength $\bar{\sigma}_t$ on pure torsion strength is evaluated. Each spring of the interface model follows the Mohr-Coulomb yield criterion (Equation 7) already introduced, with $c = \bar{\sigma}_t \tan\varphi$. Figure A1 shows the torsion strength obtained with the spring model and increasing tensile strength with a continuous line, compared with the analytic

expression of Equation (12) plotted with dashed line. Small differences are found for increasing tensile strength, due to the interface discretization.

Then, the effect of combined torsion and shear along one or both plane directions is evaluated and the shear stress lines over the interface are plotted for several intermediate cases between the pure torsion (already showed in Figure 7) and the pure shear force. Figure A2 collects stress lines in case of torsion and increasing shear force in y_1 direction, showing that the twisting centre moves towards interface centre along y_2 axis and stress lines tend to become straight and parallel to y_1 axis. Similarly, Figure A3 collects stress lines in case of torsion and increasing shear forces in both plane directions. Moreover, in order to evaluate the effects of interface dimension ratio l_1/l_2 on the torsion-shear strength domain, several incremental analyses are performed with the proposed spring model and adopting a set of values for l_1/l_2. Figure A4 collects separately the torsion-shear strength domains determined numerically and already showed in Figure 9. Given that the expression for the perfect circular shape of torsion-shear strength domain is $(m_3 / m_{3,u})^2 + (f_1 / f_{s,u})^2 \leq 1$, the corresponding curve turns out to be almost coincident with numerical results only if $l_1/l_2 = 0.5$, whereas it must be noted that in case of $l_1/l_2 = 10$, torsion-shear strength domain turns out to be well approximated by the expression $m_3 / m_{3,u} + (f_1 / f_{s,u})^2 \leq 1$. Then, a general expression for such domain may be defined as:

$$(m_3 / m_{3,u})^{\alpha} + (f_1 / f_{s,u})^2 \leq 1. \tag{A4}$$

Where exponent α depends on interface dimension ratio and converges to 1 for small values of l_1/l_2; several estimates of α are presented in the second column of Table A1; the corresponding curves are added to the domains in Figure A4 with dashed lines, showing a quite good agreement between the proposed expression and numerical results. However, it must be noted that Equation (A4) regards the simple case of combined torsion and shear along y_1 direction. In case of torsion and shear along y_2 direction, exponents α assume the values corresponding to the cases with inverse l_1/l_2 values (third column of Table A1). Moreover, the more general case with combined shear forces along y_1 and y_2 direction is characterized by α values depending also on the ratio between f_1 and f_2 and varying between the two limit cases showed in second and third column of Table A1. Then, the estimate of exponents α turns out to be more difficult than expected and for instance the simple case of interface subject to equal shear forces $f_1 = f_2$ is added to Table A1. For simplicity, it must be noted that masonry panels made of standardised bricks with regular –running bond– pattern are characterized by

horizontal interfaces having l_1/l_2 almost equal to 1 (given that in most of standardized bricks $b/s = 2$). In this case, it may be easily found that, in case of horizontal joints, exponents α do not depend on f_1/f_2 and are always equal to 1.43. In case of vertical joints, l_1/l_2 is almost equal to 0.5 ($a/s = 0.5$ for standardised bricks) and exponents α vary from 1.25 to 1.92. Then, an intermediate value of α may be assumed equal to 1.50 in the following expression for torsion strength domain as function of generic shear stresses:

$$(m_3 / m_{3,u})^{\alpha} + (f_1^2 + f_2^2) / f_{s,u}^2 \leq 1. \qquad \text{(A5)}$$

Table captions

Table 1: Limit loads obtained with DEM and reference results of the masonry panels studied by Orduña and Lourenço (2005b).

Table 2: Limit loads obtained with DEM and reference results of the masonry specimens considered by Restrepo Vélez et al. (2014).

Table 3: Dimensions, restraints, ultimate pressures obtained with DEM and reference results of several masonry specimens tested by Chee Liang (1996).

Table A1: Exponents α in Equation A5 depending on interface dimension ratio l_1/l_2 and varying shear forces.

Figure captions

Figure 1. Discrete model, a) running bond Representative Elementary Volume (REV), b) block displacements and rotations.

Figure 2: a) generic horizontal interface; b) generic vertical interface; c) generic interface with local coordinate system and interface forces and moments.

Figure 3: a) interface discretization; b) set of springs for modelling a generic interface.

Figure 4: Interface subject to relative plane displacements.

Figure 5: Incremental analyses for evaluating interface shear strength in both plane directions.

Figure 6: Interface subject to (a) relative plane rotation; (b) plane relative rotation and relative displacement.

Figure 7: Shear stress lines over the interface in case of pure torsion (a) and in case of combined torsion and shear force f_1 (b).

Figure 8: Incremental analyses for evaluating the combination of interface shear strength with interface torsion strength.

Figure 9: Dimensionless torsion-shear strength domain for varying interface dimensions ratio l_1/l_2.

Figure 10: Torsion strength-bending moments interaction curves.

Figure 11: Typical out of plane collapse mechanisms of a masonry wall with increasing restraints.

Figure 12: Case studies considered originally by Orduña and Lourenço (2005b).

Figure 13: Failure mechanisms for the masonry panels studied by Orduña and Lourenço (2005b) modelled with DEM.

Figure 14: Masonry specimen types considered in the experimental campaign by Restrepo Vélez et al (2014) (a-d); corresponding specimens modelled with DEM in present analysis (e-h).

Figure 15: Failure mechanisms for several masonry panels restrained along left column considered by Restrepo Vélez et al. (2014) modelled with DEM.

Figure 16: Failure mechanisms for several masonry panels restrained along lateral columns considered by Restrepo Vélez et al. (2014) modelled with DEM.

Figure 17: Failure mechanisms for the masonry panel loaded by a set of wooden beams and simply supported at its base considered by Restrepo Vélez et al. (2014) modelled with DEM.

Figure 18: Failure mechanisms for two masonry panels with openings restrained along lateral columns considered by Restrepo Vélez et al. (2014) modelled with DEM.

Figure 19: Masonry specimen types considered in the experimental campaign performed by Chee Liang (1996). Supported along four sides (a), supported along three sides (b).

Figure 20: Deformed configuration at collapse and corresponding damage maps for several specimens tested by Chee Liang (1996) and modelled with DEM with four simply supported sides (interface colours: green = elastic, red = shear failure, magenta = flexural failure).
Figure 21: Deformed configuration at collapse and corresponding damage maps for several specimens tested by Chee Liang (1996) and modelled with DEM with three simply supported and one free side (interface colours: green = elastic, red = shear failure, magenta = flexural failure).
Figure 22: Lateral pressure-out of plane displacement pushover curves for several specimens originally tested by Chee Liang (1996) and modelled with DEM.

Figure A1: Torsion strength as function of interface tensile strength. Continuous line for numerical results with the proposed spring model, dashed line for analytic expression (Equation 12).
Figure A2: Stress lines for combined torsion and shear force along y_1 direction.
Figure A3: Stress lines for combined torsion and shear forces along y_1 and y_2 directions.
Figure A4: Dimensionless torsion-shear strength domains varying interface dimensions ratio l_1/l_2

Figure

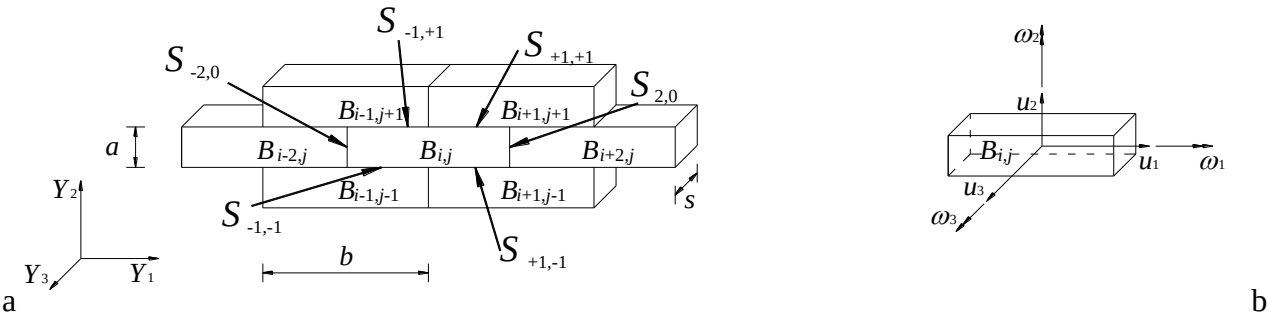

Figure 1. Discrete model, a) running bond Representative Elementary Volume (REV), b) block displacements and rotations.

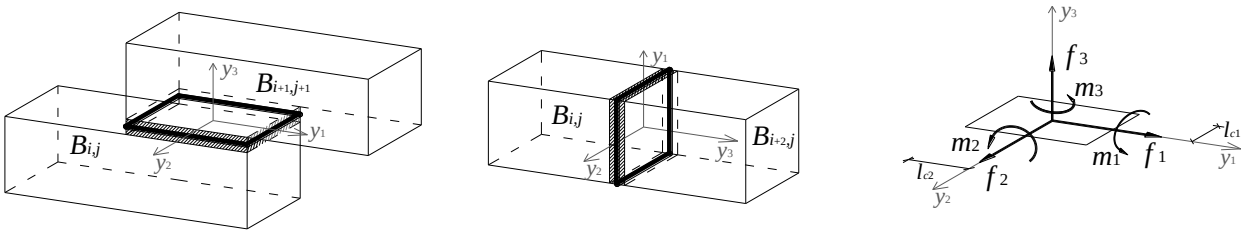

Figure 2: a) generic horizontal interface; b) generic vertical interface; c) generic interface with local coordinate system and interface forces and moments.

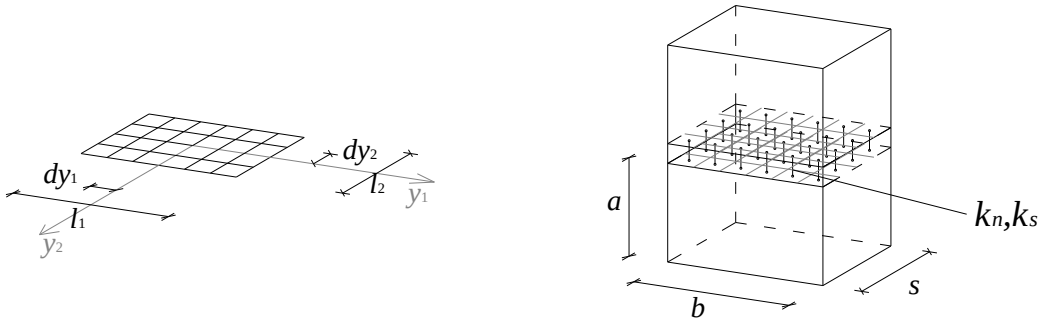

a b

Figure 3: a) interface discretization; b) set of springs for modelling a generic interface.

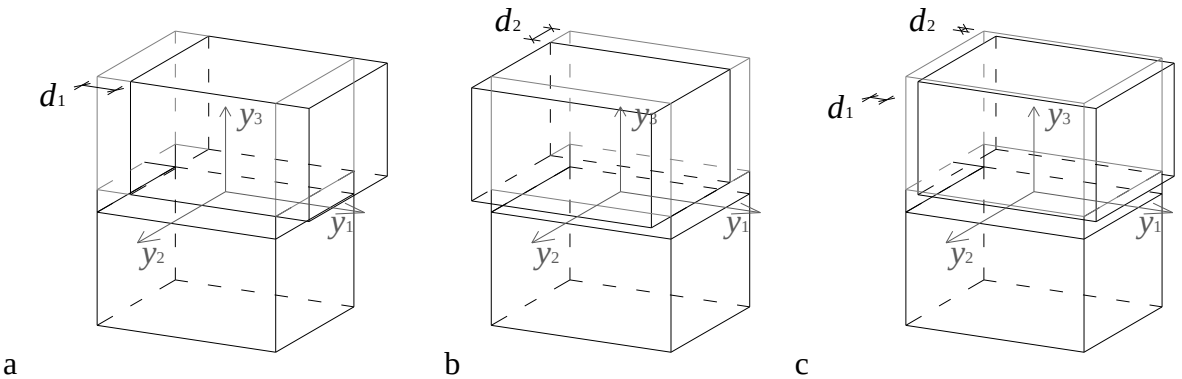

Figure 4: Interface subject to relative plane displacements.

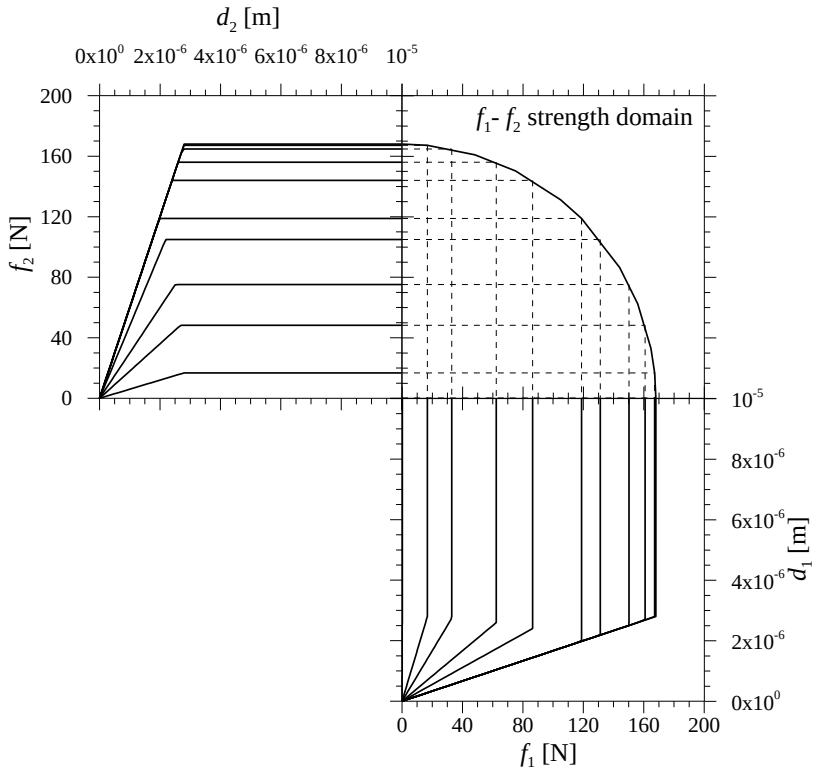

Figure 5: Incremental analyses for evaluating interface shear strength in both plane directions.

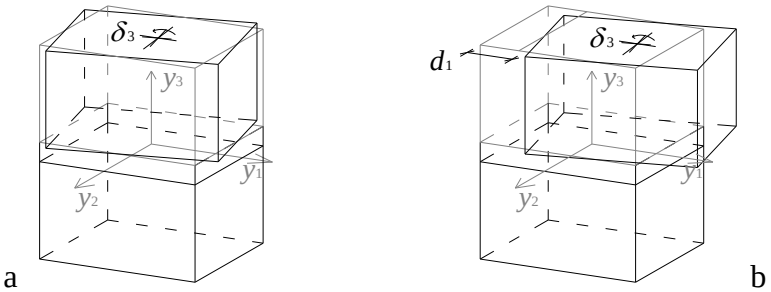

Figure 6: Interface subject to (a) relative plane rotation; (b) plane relative rotation and relative displacement.

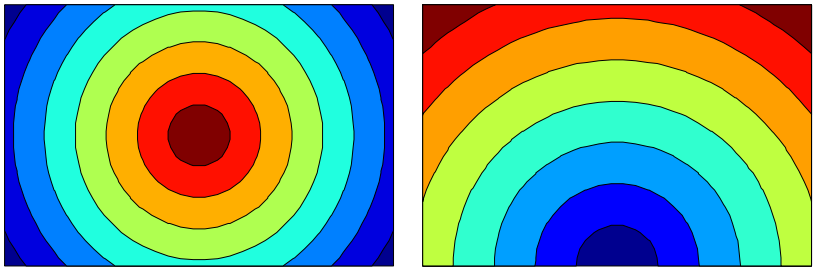

a b

Figure 7: Shear stress lines over the interface in case of pure torsion (a) and in case of combined torsion and shear force f_1 (b).

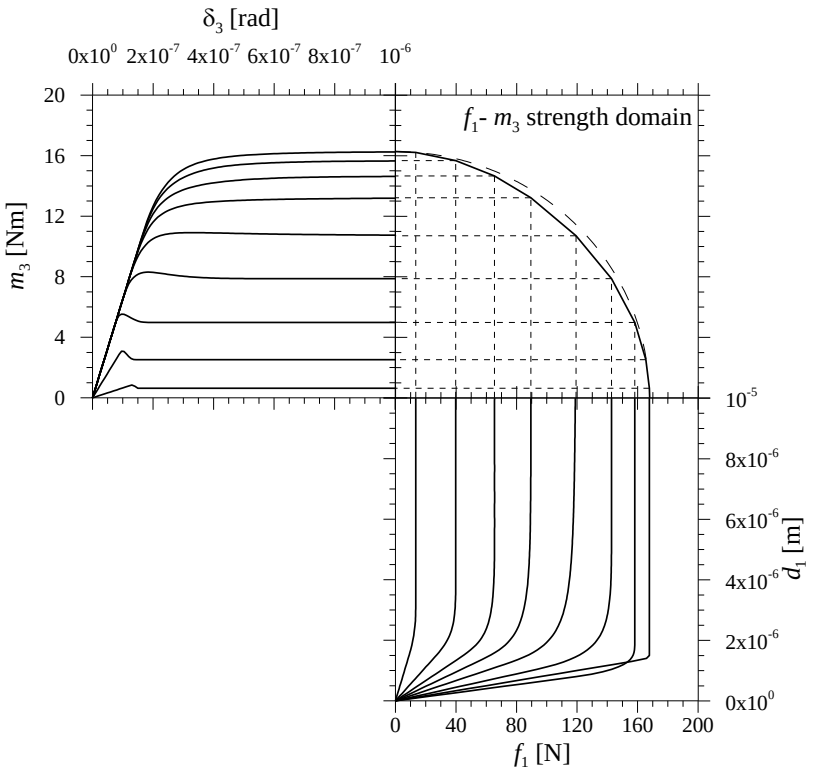

Figure 8: Incremental analyses for evaluating the combination of interface shear strength with interface torsion strength.

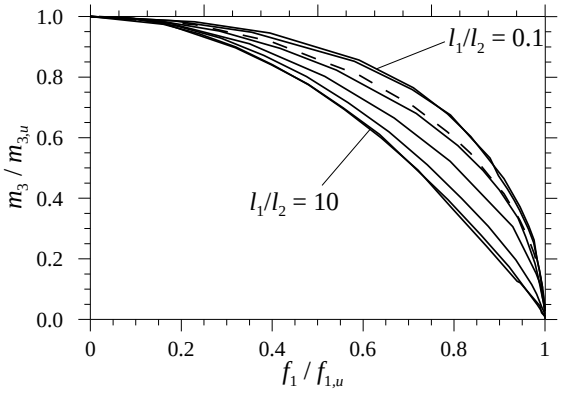

Figure 9: Dimensionless torsion-shear strength domain varying interface dimensions ratio l_1/l_2.

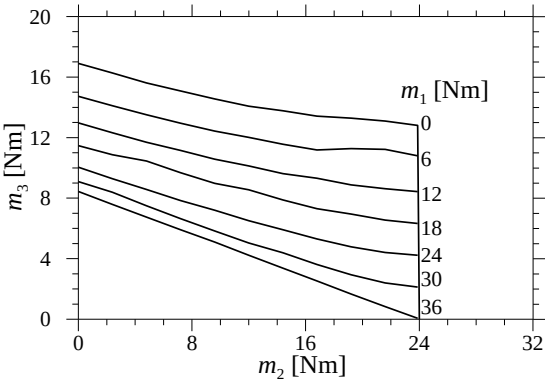

Figure 10: Torsion strength-bending moments interaction curves.

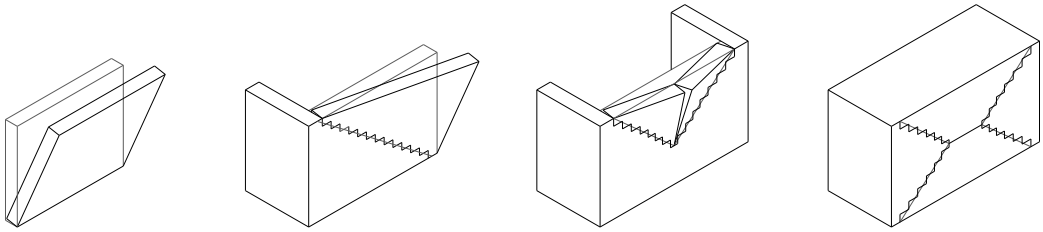

Figure 11: Typical out of plane collapse mechanisms of a masonry wall with increasing restraints.

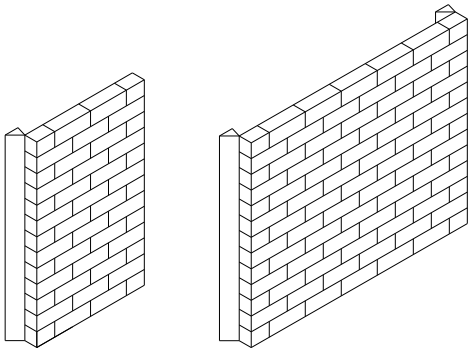

a b

Figure 12: Case studies considered originally by Orduña and Lourenço (2005b)

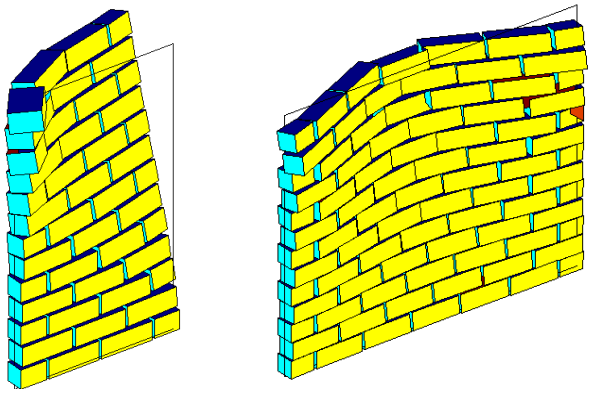

a b

Figure 13: Failure mechanisms for the masonry panels studied by Orduña and Lourenço (2005b) modelled with DEM.

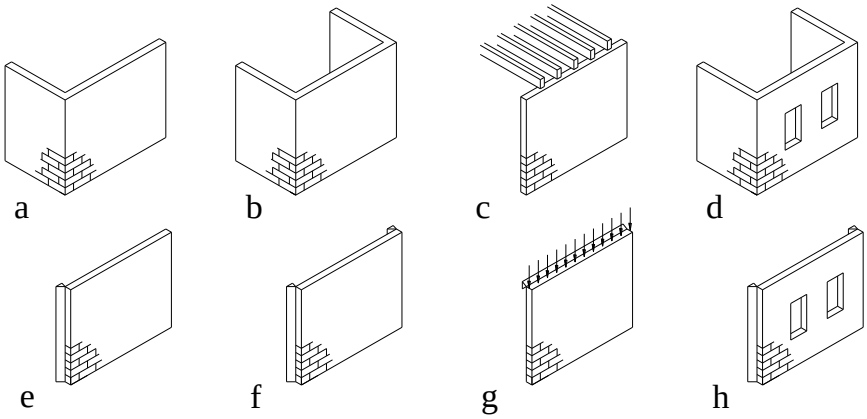

Figure 14: Masonry specimen types considered in the experimental campaign by Restrepo Vélez et al (2014) (a-d); corresponding specimens modelled with DEM in present analysis (e-h).

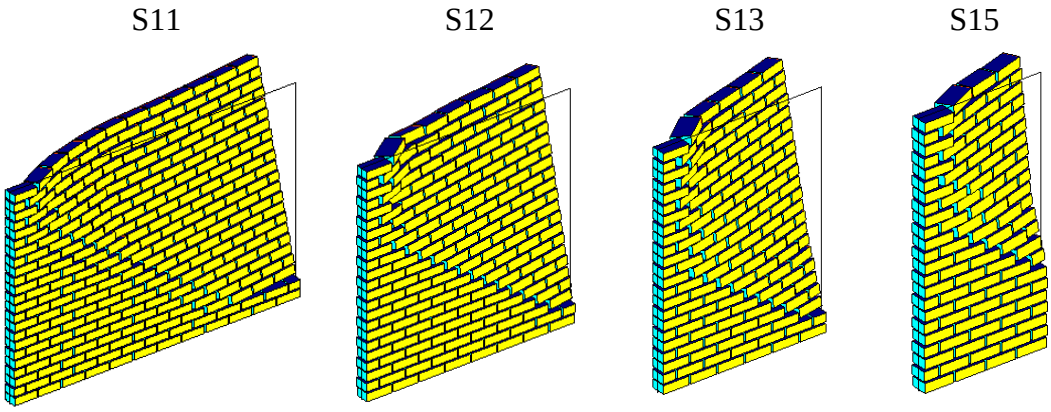

Figure 15: Failure mechanisms for several masonry panels restrained along left column considered by Restrepo Vélez et al. (2014) modelled with DEM.

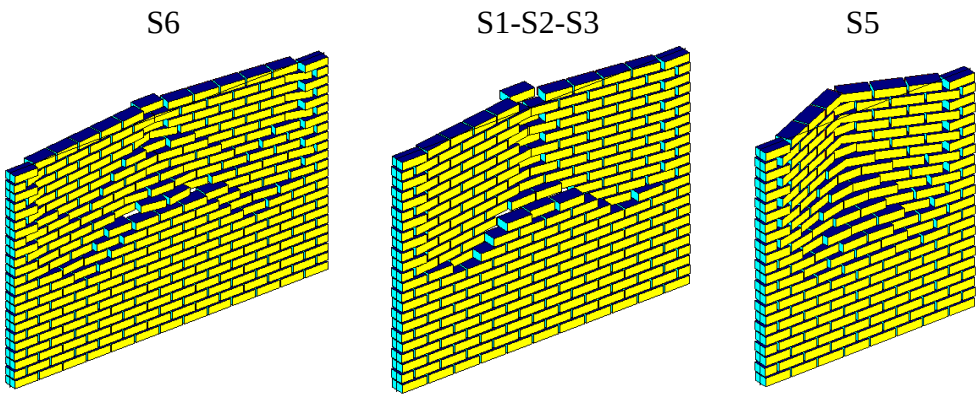

Figure 16: Failure mechanisms for several masonry panels restrained along lateral columns considered by Restrepo Vélez et al. (2014) modelled with DEM.

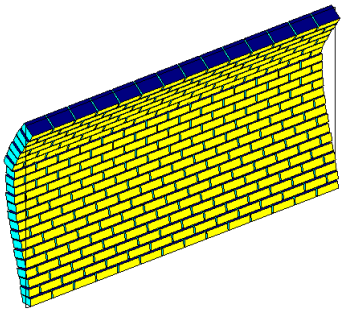

Figure 17: Failure mechanism for the masonry panel loaded by a set of wooden beams and simply supported at its base considered by Restrepo Vélez et al. (2014) modelled with DEM.

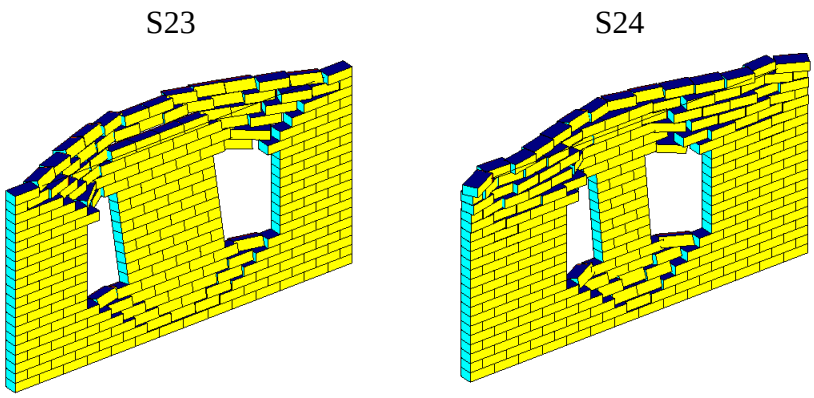

Figure 18: Failure mechanisms for two masonry panels with openings restrained along lateral columns considered by Restrepo Vélez et al. (2014) modelled with DEM.

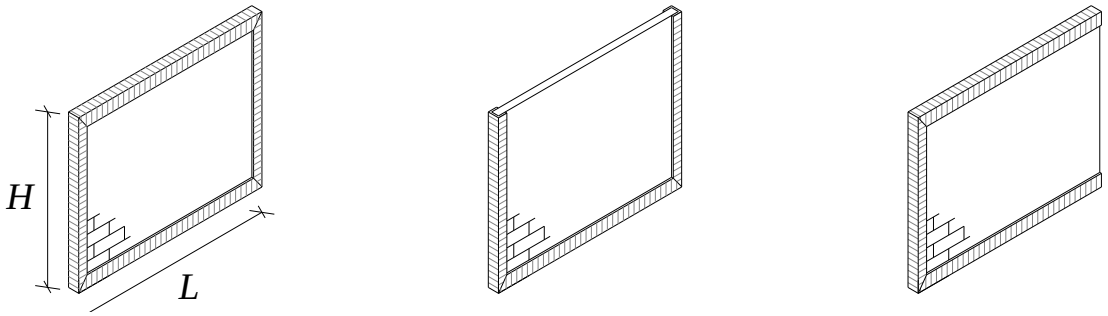

Figure 19: Masonry specimen types considered in the experimental campaign performed by Chee Liang (1996).

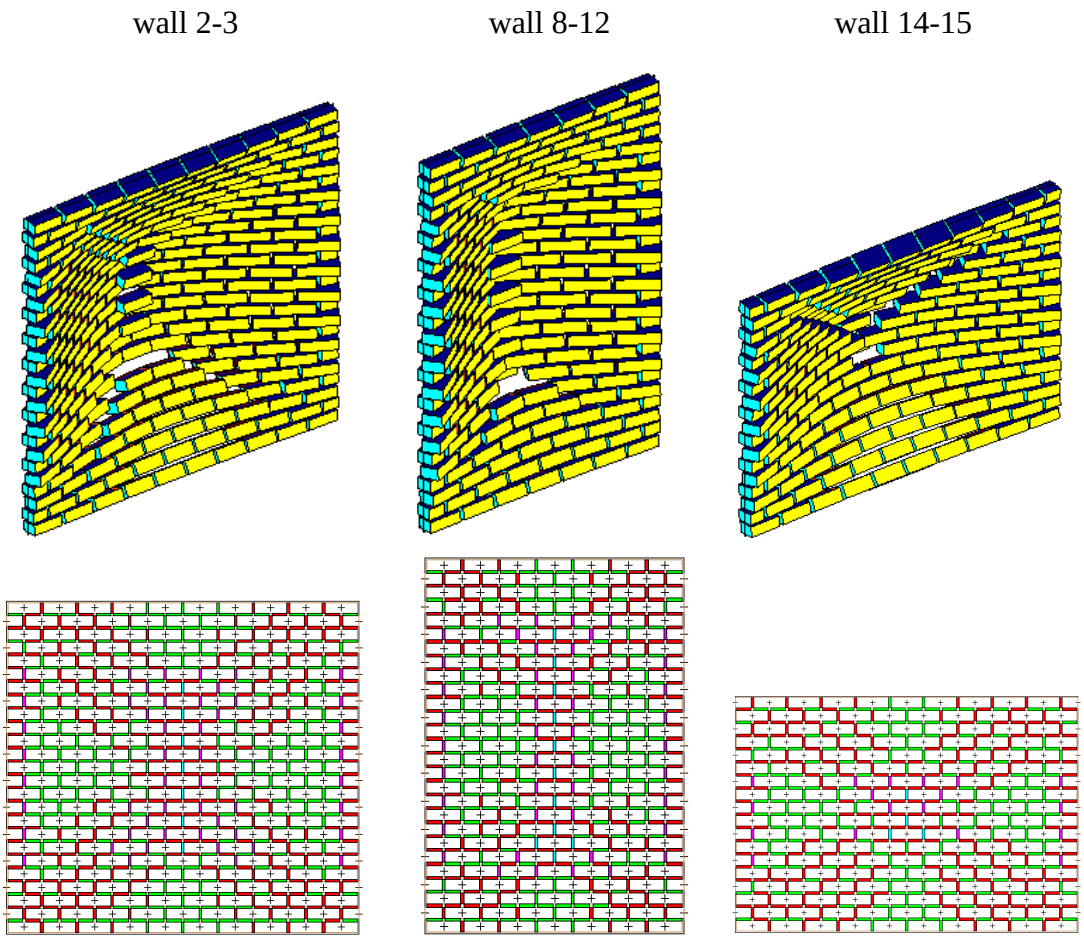

Figure 20: Deformed configuration at collapse and corresponding damage maps for several specimens tested by Chee Liang (1996) and modelled with DEM with four simply supported sides (interface colours: green = elastic, red = shear failure, magenta = flexural failure).

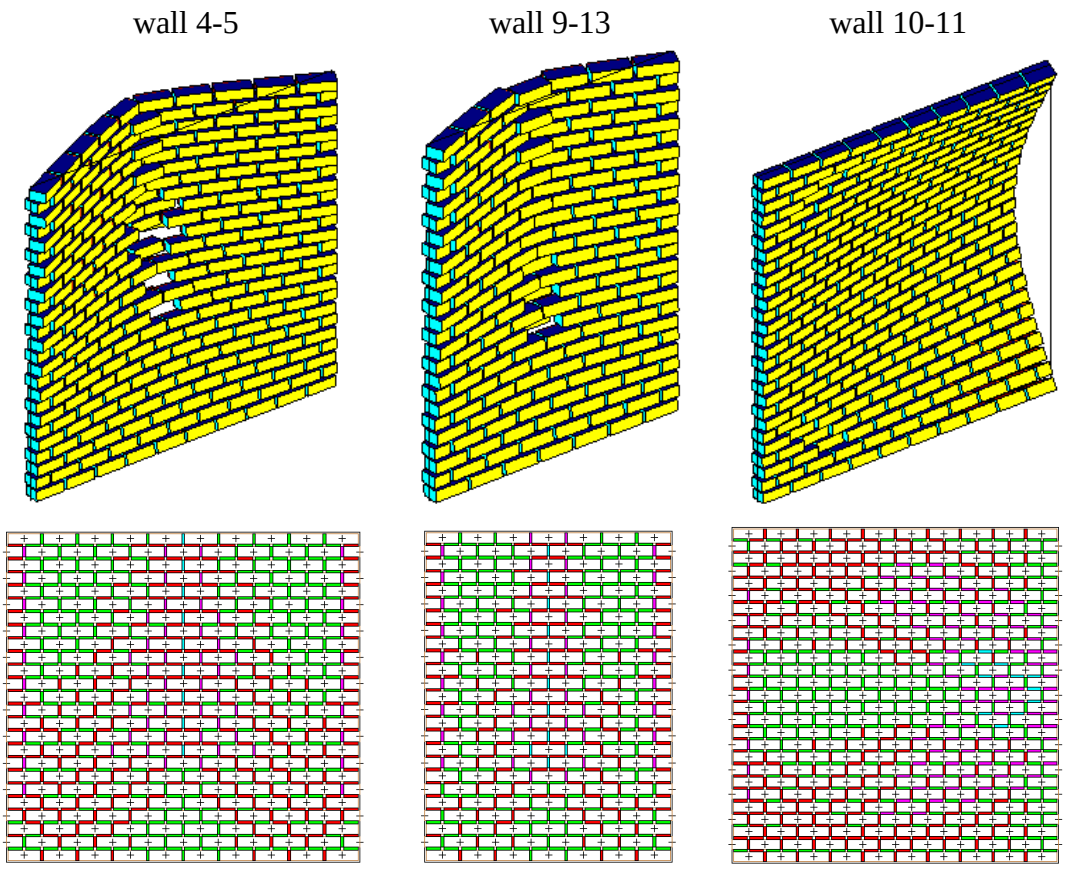

Figure 21: Deformed configuration at collapse and corresponding damage maps for several specimens tested by Chee Liang (1996) and modelled with DEM with three simply supported and one free side (interface colours: green = elastic, red = shear failure, magenta = flexural failure).

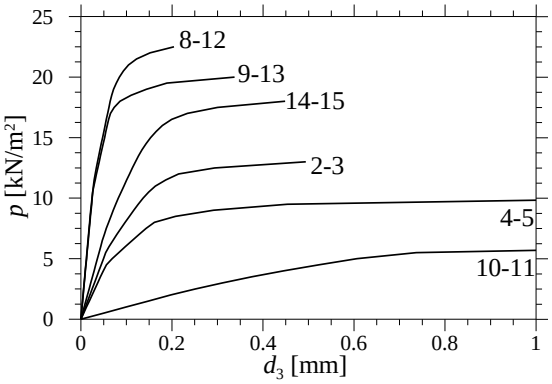

Figure 22: Lateral pressure-out of plane displacement pushover curves for several specimens originally tested by Chee Liang (1996) and modelled with DEM.

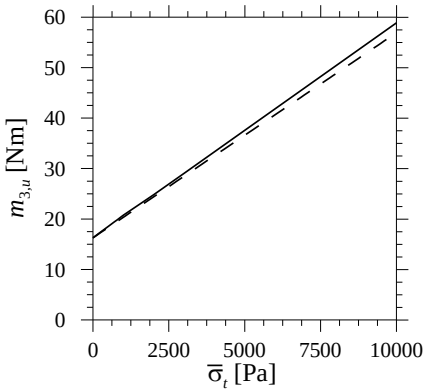

Figure A1: Torsion strength as function of interface tensile strength. Continuous line for numerical results with the proposed spring model, dashed line for analytic expression (Eq. 12).

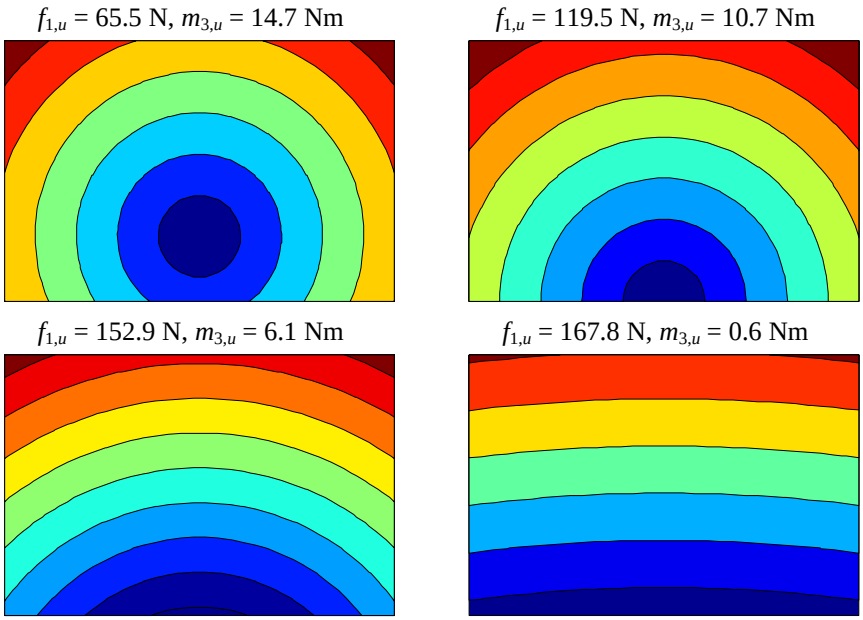

Figure A2: Stress lines for combined torsion and shear force along y_1 direction.

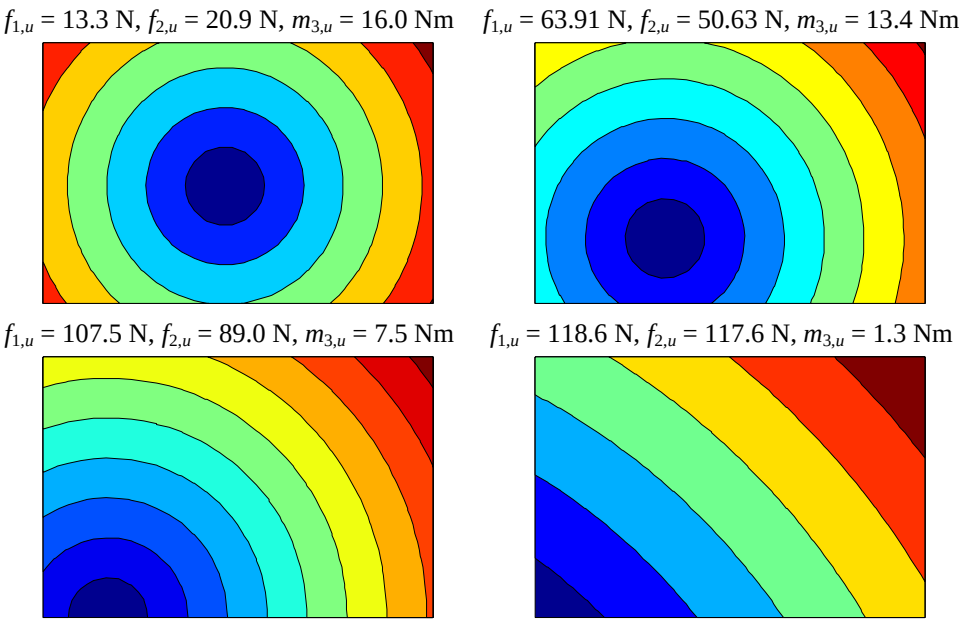

Figure A3: Stress lines for combined torsion and shear forces along y_1 and y_2 directions.

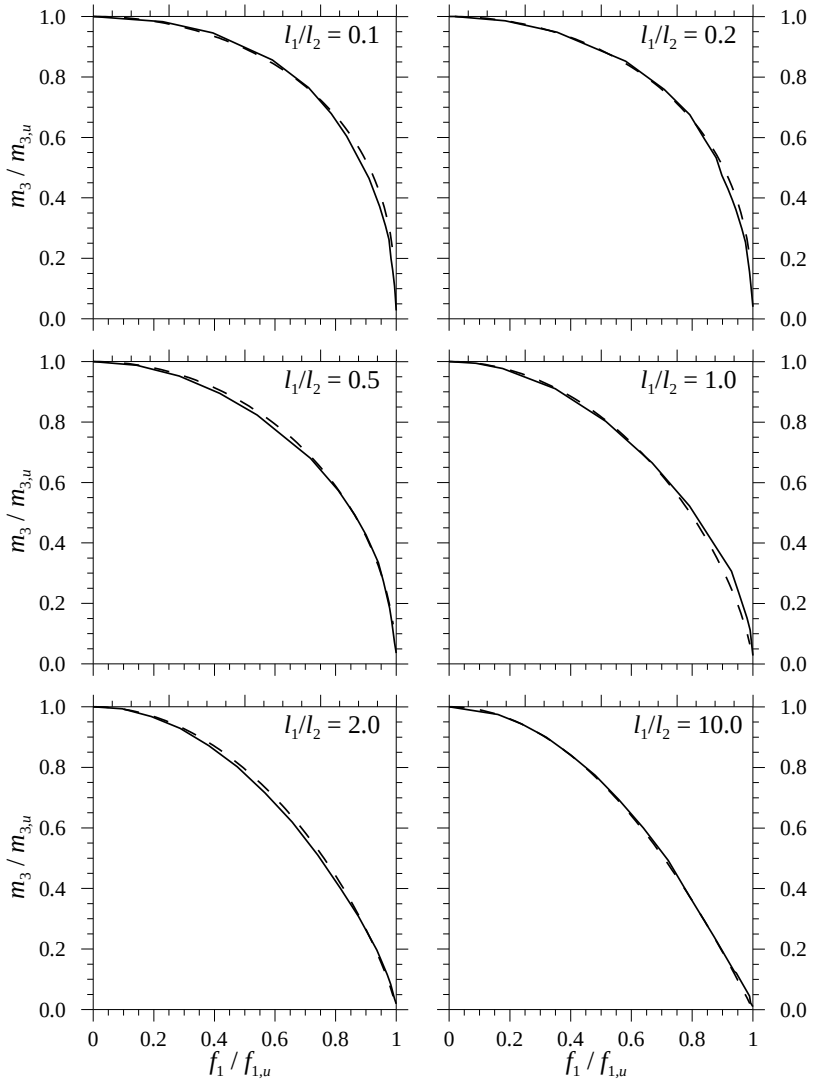

Figure A4: Dimensionless torsion-shear strength domains varying interface dimensions ratio l_1/l_2

Tables

case	1	2
λ^{DEM}	0.175	0.215
$\lambda^{REF,FEM}$	0.210	0.260
$\lambda^{REF,lim}$	0.127	0.193

Table 1: Limit loads obtained with DEM and reference results of the masonry panels studied by Orduña and Lourenço (2005b).

specimen	S11	S12	S13	S15	S6	S1-S2-S3	S5	S32	S23	S34
n	12	8	6	4	13	11	8	14	14	14
λ^{DEM}	0.100	0.125	0.165	0.250	0.160	0.225	0.350	0.305	0.130	0.140
λ^{REF}	0.097	0.129	0.181	0.199	0.208	0.208	0.349	0.293	0.144	0.156

Table 2: Limit loads obtained with DEM and reference results of the masonry specimens considered by Restrepo Vélez et al. (2014).

wall	2-3	8-12	14-15	4-5	9-13	10-11
L [m]	1.15	0.795	1.130	1.14	0.795	1.20
H [m]	1.15	1.190	0.755	1.14	1.140	1.20
restraint		4 sides		3 sides, free top		3 sides, free left
p^{DEM} [kN/m^2]	13.00	25.0	18.0	10.00	20.0	6.5
p^{REF} [kN/m^2]	12.20	25.0	20.6	8.54	23.5	5.20
	12.55	31.8	18.9	8.55	27.8	4.51

Table 3: Dimensions, restraints, ultimate pressures obtained with DEM and reference results of several masonry specimens tested by Chee Liang (1996).

l_1/l_2	α ($f_1 \neq 0, f_2 = 0$)	α ($f_1 = 0, f_2 \neq 0$)	α ($f_1 = f_2 \neq 0$)
0.1	1.00	2.56	2.00
0.2	1.05	2.44	1.90
0.5	1.25	1.92	1.70
1.0	1.43	1.43	1.43
2.0	1.92	1.25	1.70
5.0	2.44	1.05	1.90
10.0	2.56	1.00	2.00

Table A1: Exponents α in Equation A5 depending on interface dimension ratio l_1/l_2 and varying shear forces.